

Late Triassic Granites From the Quxu Batholith Shedding a New Light on the Evolution of the Gangdese Belt in Southern Tibet

MENG Yuanku^{1,2,3}, XU Zhiqin^{4,5,*}, XU Yang³ and MA Shiwei⁴

1 College of Earth Science and Engineering, Shandong University of Science and Technology, Qingdao 266590, Shandong, China

2 Key Laboratory of Depositional Mineralization and Sedimentary Mineral of Shandong province, Qingdao 266590, Shandong, China

3 Qingdao Institute of Marine Geology, China Geological Survey, Qingdao 266061, China

4 Institute of Geology, Chinese Academy of Geological Sciences, Beijing 100037, China

5 School of Earth Sciences and Engineering, Nanjing University, Nanjing 210023, China

Abstract: The Gangdese magmatic belt formed during Late Triassic to Neogene in the southernmost Lhasa terrane of the Tibetan plateau. It is interpreted as a major component of a continental margin related to the northward subduction of the Neo-Tethys oceanic slab beneath Eurasia and it is the key in understanding the tectonic framework of southern Tibet prior to the India-Eurasia collision. It is widely accepted that northward subduction of the Neo-Tethys oceanic crust formed the Gangdese magmatic belt, but the occurrence of Late Triassic magmatism and the detailed tectonic evolution of southern Tibet are still debated. This work presents new zircon U-Pb-Hf isotope data and whole-rock geochemical compositions of a mylonitic granite pluton in the central Gangdese belt, southern Tibet. Zircon U-Pb dating from two representative samples yields consistent ages of 225.3 ± 1.8 Ma and 229.9 ± 1.5 Ma, respectively, indicating that the granite pluton was formed during the early phase of Late Triassic instead of Early Eocene (47–52 Ma) as previously suggested. Geochemically, the mylonitic granite pluton has a sub-alkaline composition and low-medium K calc-alkaline affinities and it can be defined as an I-type granite with metaluminous features ($A/CNK < 1.1$). The analyzed samples are characterized by strong enrichments of LREE and pronounced depletions of Nb, Ta and Ti, suggesting that the granite was generated in an island-arc setting. However, the use of tectonic discrimination diagrams indicates a continental arc setting. Zircon Lu-Hf isotopes indicate that the granite has highly positive $\epsilon_{\text{Hf}}(t)$ values ranging from +13.91 to +15.54 (mean value +14.79), reflecting the input of depleted mantle material during its magmatic evolution, consistent with $\text{Mg}^\#$ numbers. Additionally, the studied samples also reveal relatively young Hf two-stage model ages ranging from 238 Ma to 342 Ma (mean value 292 Ma), suggesting that the pluton was derived from partial melting of juvenile crust. Geochemical discrimination diagrams also suggest that the granite was derived from partial melting of the mafic lower crust. Taking into account both the spatial and temporal distribution of the mylonitic granite, its geochemical fingerprints as well as previous studies, we propose that the northward subduction of the Neo-Tethys oceanic slab beneath the Lhasa terrane had already commenced in Late Triassic (~230 Ma), and that the Late Triassic magmatic events were formed in an active continental margin that subsequently evolved into the numerous subterranean, paleo-island-arcs and multiple collision phases that form the present southern Tibet.

Key words: Late Triassic, Neo-Tethys Ocean, active continental margin, Gangdese batholith, southern Tibet

1 Introduction

Granites and related mafic rocks play important roles in

the understanding of mantle partial melting and crust-mantle interactions. The petrogenesis of granitic rocks is, therefore, the key to studying the growth and evolution of the continental crust (Wang Tao et al., 2017). Additionally, the composition of granites can also reflect

* Corresponding author. E-mail: ykmeng@foxmail.com

the tectonic setting in which the parental melts were generated (Pitcher, 1979; Pearce et al., 1984; Maniar and Piccoli, 1989; Barbarin, 1999; Wang Tao et al., 2017). Negative $\varepsilon_{\text{Hf}}(t)$ values and old model ages suggest the partial melting of pre-existing crustal materials. By contrast, positive $\varepsilon_{\text{Hf}}(t)$ values and young model ages suggest the recycling of juvenile crust or the input of nascent mantle material (Vervoort and Blichert-Toft, 1999; Wu Fuyuan et al., 2007; Ji et al., 2009).

The Gangdese magmatic belt, located in Tibet at the southern margin of the Lhasa terrane, records vital information on the subduction of the Neo-Tethys oceanic slab and the subsequent Indian-Asian collision (Chung et al., 2003, 2005; Wen et al., 2008; Ji et al., 2009; Ji Weiqiang et al., 2009; Mo Xuanxue et al., 2009; Zhu et al., 2011, 2015; Huang Yong et al., 2017). Previous studies mainly focus on the Cretaceous and Cenozoic magmatic events (Jin Chengwei and Zhou Yunsheng, 1978; Tu Guangchi et al., 1981; Xu Ronghua and Jin Chengwei, 1984; Chung et al., 2003, 2005; Mo Xuanxue et al., 2003, 2005a,b, 2009; Mo et al., 2008; Ji et al., 2009; Huang Yu et al., 2010; Mo Xuanxue, 2011; Zhu et al., 2011, 2015; Wang et al., 2015; Xu et al., 2015; Ma et al., 2016; Ma et al., 2017; and references therein), involving petrology, geochronology, geochemistry and isotope geology. It is widely accepted that the Neo-Tethys oceanic slab subducted beneath the Lhasa terrane during Early Cretaceous and formed the well-known Gangdese magmatic belt, as reflected by strong magmatic activities during this period (Yin and Harrison, 2000; Mo et al., 2008; Mo Xuanxue, 2011; Zhu et al., 2011, 2015).

However, the occurrence of rare pre-Cretaceous igneous rocks in the Gangdese magmatic belt is still debate (He Zhonghua et al., 2005, 2006; Geng Quanru et al., 2006; Ji et al., 2009; Ji Weiqiang et al., 2009; Zhu et al., 2011; Song Shaowei et al., 2014; Wang Cheng et al., 2014; Meng et al., 2016a, b; Wang et al., 2016; Ma et al., 2017; Xu Bo et al., 2017). Some researchers argue that the pre-Cretaceous magmatic rocks are the products of subducted Neo-Tethys oceanic plate (Ji et al., 2009; Ji Weiqiang et al., 2009; Peng Jianhua et al., 2013; Meng et al., 2016a, b; Wang et al., 2016; Ma et al., 2017), while others suggest them to be related to the southward subduction of the Bangong-Nujiang oceanic crust (Geng Quanru et al., 2006; Zhu et al., 2011; Song Shaowei et al., 2014; Wang Cheng et al., 2014). By contrast to these models, other workers imply that the pre-Cretaceous magmatic activities could be associated with the evolution of the Paleo-Tethys oceanic crust and related to the Songduo oceanic slab break-off (Dong Xin and Zhang Zeming, 2013) as well as Early Indosinian orogenic events (Zhang Hongfei et al., 2007; Li Huaqi, 2009).

In this paper, we report new zircon U-Pb data, Lu-Hf isotopes and whole-rock major and trace element data for the mylonitic granite in the Quxu region, southern Tibet, enabling us to consider new age information and to better define the intrusive activity in the central Gangdese magmatic belt. Our results, in combination with published data from previous workers, further support the hypothesis that the subduction of the Neo-Tethys oceanic slab beneath the Lhasa terrane had already commenced before Late Triassic (~230 Ma) and, hence, southern Tibet might have evolved along a continental margin. This study bears significant implications not only for the petrogenesis of the mylonitic granite, but also for the early tectonic evolution of southern Tibet.

2 Geological Setting and Samples

From south to north (Fig. 1a), the Tibetan plateau consists of the Himalaya, Lhasa, Qiangtang, Songpan-Ganzi, and Qaidam terranes, which are separated by the Indus-Yarlung Tsangpo suture zone (IYTSZ), the Bangong-Nujiang suture zone (BNSZ) and the Jinsha suture zone (JSSZ), respectively (Li Cai, 1987; Yin and Harrison, 2000; Xu Zhiqin et al., 2011; Zhu et al., 2011; Meng Yuanku et al., 2016a). The Lhasa terrane, located between the IYTSZ and BNSZ, represents the southernmost Eurasian plate which has separated from Gondwanaland during Late-Permian or Early Triassic and drifted northward across the Paleo-Tethys Ocean before it collided with the northern Eurasian plate along the BNSZ during the Early Cretaceous (Yin and Harrison, 2000; Zhu et al., 2011; Pan et al., 2012; Meng Yuanku et al., 2016b; Zhang et al., 2017). Regional faults, tectonic mélanges and ultra-high pressure (UHP) rocks (e.g., the Songduo eclogite) divide the Lhasa terrane into three sub-terrane: the south-Lhasa sub-terrane (SL), the central-Lhasa sub-terrane (CL) and the north-Lhasa sub-terrane (NL) (Fig. 1a). These sub-terrane are separated by the Shiquan River-Nam Tso mélangé zone and the Luobadui-Milashan fault from the north to the south (Fig. 1a) (Yang et al., 2006; Mo Xuanxue et al., 2009; Zhu et al., 2011).

The south-Lhasa sub-terrane, located in the southern region of the LMF and covering > 80 volume percent of the igneous rocks in the entire Tibet region (Fig. 1b), is also known as the Gangdese magmatic belt, which extends from Kailas Mountain in the west to Nyingchi city in the east. The rock types of the Gangdese magmatic belt are mainly composed of diorites, granodiorites, monzogranites and syenogranites, as well as a small number of gabbroic complexes (Ji Weiqiang et al., 2009; Mo Xuanxue et al., 2009; Xu Wangchun, 2010; Qiu Jiansheng et al., 2015). The granitic rocks exposed in the Gangdese belt are well

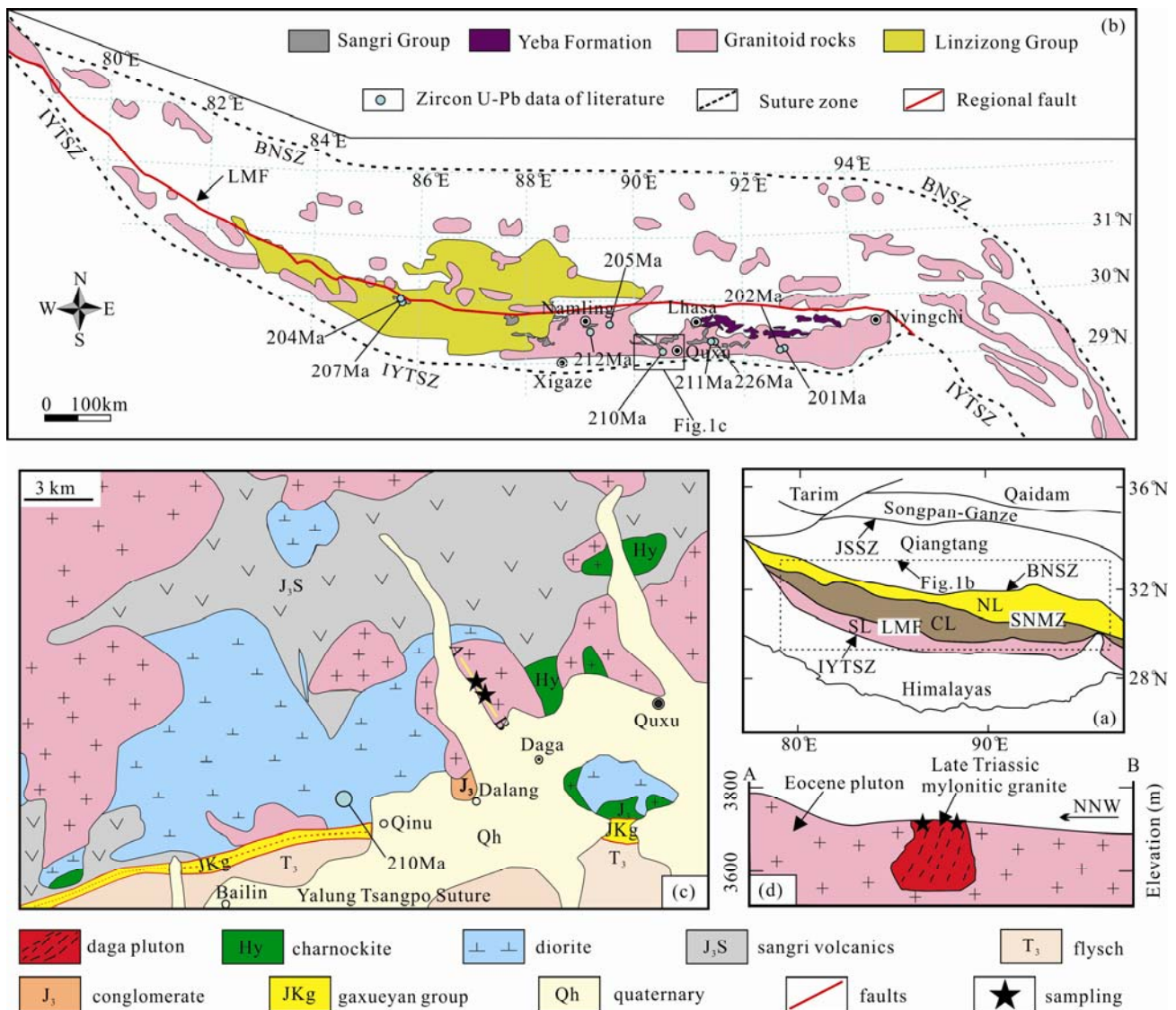


Fig. 1. (a), Tectonic units of the Tibetan plateau (Yin and Harrison, 2000; Zhu et al., 2011). (b), Mesozoic-Cenozoic igneous rocks distribution of the Lhasa terrane (after Wang et al., 2016); Ages for Late Triassic magmatic rocks are from reference: Chu et al. (2006), He Zhonghua et al. (2006), Geng Quanru et al. (2006), Ji et al. (2009), Zhu et al. (2011), Peng Jianhua et al. (2013), Song Shaowei et al. (2014), Meng et al. (2016a), Wang et al. (2016), Ma et al. (2017). (c), Simplified geological map of the Quxu region (modified from 1:25,000 geological map). (d), Schematic cross section across line A-B shown in panel (c).

JSSZ-Jinsha suture zone; LSSZ-Longmu Co-Shuanghu suture zone; BNSZ-Bangong-Nujiang suture zone; IYTSZ-Indus-Yarlung Tsangpo suture zone; SNMZ-Shiquan River-Nam Tso Mélange zone; LMF-Luobadui-Milashan fault; NL-north Lhasa terrane; CL-central Lhasa terrane; SL-south Lhasa terrane.

documented, especially their geochronological framework, as well as their whole-rock geochemical and isotope compositions. Based on previous studies, Ji Weiqiang et al. (2009) identify four stages of magmatic activities in the Gangdese batholith during the periods of 205–152 Ma, 109–80 Ma, 65–41 Ma and 33–13 Ma, respectively.

The Cretaceous and Cenozoic granites are widely distributed throughout the Gangdese belt, and they represent main components (Ji et al., 2009; Zhu et al., 2011; Ma et al., 2016). Jurassic and Late Triassic igneous rocks are also recorded in the Gangdese belt (Chu et al., 2006; Geng Quanru et al., 2006; Zhang Hongfei et al., 2007; Ji Weiqiang et al., 2009; Zhu et al., 2011; Kang et

al., 2014; Qiu Jiansheng et al., 2015; Wang et al., 2016; Meng et al., 2016a,b; Ma et al., 2017; and references therein) (Fig. 1b). They consist of rhyolites, granitoids and hornblende-gabbros, all with arc-related geochemical signatures (Ji et al., 2009; Ji Weiqiang et al., 2009; Meng et al., 2016a,b; Wang et al., 2016; Ma et al., 2017). However, the detailed petrogenesis and tectonic setting of these pre-Cretaceous igneous rocks remain controversial and poorly understood (Geng Quanru et al., 2006; Zhang Hongfei et al., 2007; Ji et al., 2009; Zhu et al., 2011; Dong Xin and Zhang Zeming, 2013; Meng et al., 2016a,b; Wang et al., 2016; Ma et al., 2017; and references therein).

Our study area lies adjacent to the Daga township of

Quxu County, with a good infrastructure (Fig. 1c). In the text below, we refer to the mylonitic granite pluton as the Daga pluton. The Daga pluton forms part of the Quxu batholith (Fig. 1d). We collected nine representative samples of the Daga pluton, including two samples for zircon LA-ICP-MS U-Pb dating and seven samples for whole-rock geochemistry. The detailed sample locations (GPS) are listed in Table 1.

Petrographic thin section studies reveal that the granite experienced ductile deformation and structural shearing, corresponding to our field observations (Fig. 2a–b). The Daga granite mainly consists of quartz (25–30%), plagioclase (~30%), K-feldspar (~25%), hornblende (5–10%) with minor sericite, chlorite, and accessory minerals (zircon, apatite, allanite and magnetite). Quartz grains display ductile deformation, marked by undulating extinction, sub-grain rotation and zoning; besides, some grains comprise banded structures suggesting moderate to low temperature deformation processes (Fig. 2c–f). However, feldspar crystals show brittle deformation in places and a weak clay-sericite alteration (Fig. 2c–f), characterized by typical cellular and locally turbid textures. Hornblende grains have greenish colors and form elongated crystals, indicating a primary magmatic origin. In summary, the Daga pluton only experienced very weak alteration and weathering.

3 Analytical Methods

3.1 Zircon U-Pb dating analyses

The selection of zircons for this study was completed at the Mineral Laboratory of Hebei Province Geological Survey. The detailed steps were as follows: two granite samples (each one for ~2.5 kg) were pulverized, and then separated by liquid and magnetic techniques. Subsequently, we picked idiomorphic zircons under the binocular. All selected zircons were pristine and without ruptures. Finally, the selected zircons were fixed on the epoxy resin, and then polished for analyses. The

Cathodoluminescence (CL) images were taken at the CL laboratory of Key Laboratory of Continental Tectonics and Dynamics (KLCTD), Institute of Geology, Chinese Academy of Geological Sciences (CAGS).

The zircon U-Pb dating analyses were conducted at the State Key Laboratory of Mineral Deposits Research (SKLMDR), Nanjing University. The analytical instrument was a Geolas2005 laser ablation system and an Agilent 7500a Inductively Coupled Plasma Mass Spectrometer (ICP-MS) using a laser spot diameter of about 35 μm . The carrier gas was Helium; the gas flow rate was 270 mL/min; the working voltage was 27.1 kv, and the energy of the laser ablation was about 29 J/ cm^2 . GEMOC GJ-1 Standards were used for isotopic calibrations, and Mud Tank was used for accuracy verification. The detailed analytical methods are documented by Griffin et al. (2004) and Jackson et al. (2004), respectively. The data were processed using the Glitter (ver.4.4) software for isotopic ratios and U-Pb ages corrections. The concordia diagrams and weighted age calculations were performed by the Isoplot software (ver.4.11) (Ludwig, 2001).

3.2 Zircon Lu-Hf isotopic analyses

The Lu-Hf isotopic analyses of zircons were carried out at the SKLMDR, Nanjing University. The experiments were conducted on the Nu Plasma HR Multi-Received Inductively Coupled Plasma Mass Spectrometer (MC-ICP-MS). The zircon standard 91500 has a $^{176}\text{Hf}/^{177}\text{Hf}$ value of 0.282308 ± 12 , which is consistent with the value obtained by the solution method of 0.282302 ± 8 within the uncertainties (Goolaerts et al., 2004). The detailed analytical procedures of zircon Lu-Hf isotopes are described by Wu Fuyuan et al. (2007).

3.3 Whole-rock major and trace element analyses

The whole-rock geochemical analyses were completed at the Minerals-ALS Chemex, Guangzhou, China. Specific steps are described below. The analytical samples were

Table 1 GPS sample locations from the Daga granite pluton in the Quxu region, southern Tibet

Sample No.	GPS data of sampling in the Daga pluton			Rock mass	Lithology	Notes
	Latitude	Longitude	Elevation(m)			
XG1210	29°22'00.78"	90°38'26.79"	3763	Quxu batholith	mylonitic granite	U-Pb dating
XG1284	29°22'09.74"	90°38'22.04"	3767	Quxu batholith	mylonitic granite	U-Pb dating
XG1210-1	29°21'88.78"	90°38'40.34"	3780	Quxu batholith	mylonitic granite	Geochemistry
XG1210-2	29°22'00.78"	90°38'26.01"	3760	Quxu batholith	mylonitic granite	Geochemistry
XG1210-3	29°22'00.78"	90°38'22.11"	3750	Quxu batholith	mylonitic granite	Geochemistry
XG1284-1	29°22'14.84"	90°38'10.04"	3780	Quxu batholith	mylonitic granite	Geochemistry
XG1284-2	29°22'19.00"	90°38'11.01"	3760	Quxu batholith	mylonitic granite	Geochemistry
XG1284-3	29°22'08.79"	90°38'55.03"	3780	Quxu batholith	mylonitic granite	Geochemistry
XG1284-4	29°22'09.74"	90°38'22.04"	3750	Quxu batholith	mylonitic granite	Geochemistry
XG1210-4	29°22'00.78"	90°38'26.79"	3769	Quxu batholith	mylonitic granite	Thin section
XG1284-5	29°22'01.52"	90°38'22.04"	3754	Quxu batholith	mylonitic granite	Thin section
XG1284-6	29°22'09.74"	90°38'30.00"	3755	Quxu batholith	mylonitic granite	Thin section
XG1284-7	29°22'09.74"	90°38'22.04"	3763	Quxu batholith	mylonitic granite	Thin section
XG1284-8	29°22'12.10"	90°38'25.16"	3761	Quxu batholith	mylonitic granite	Thin section

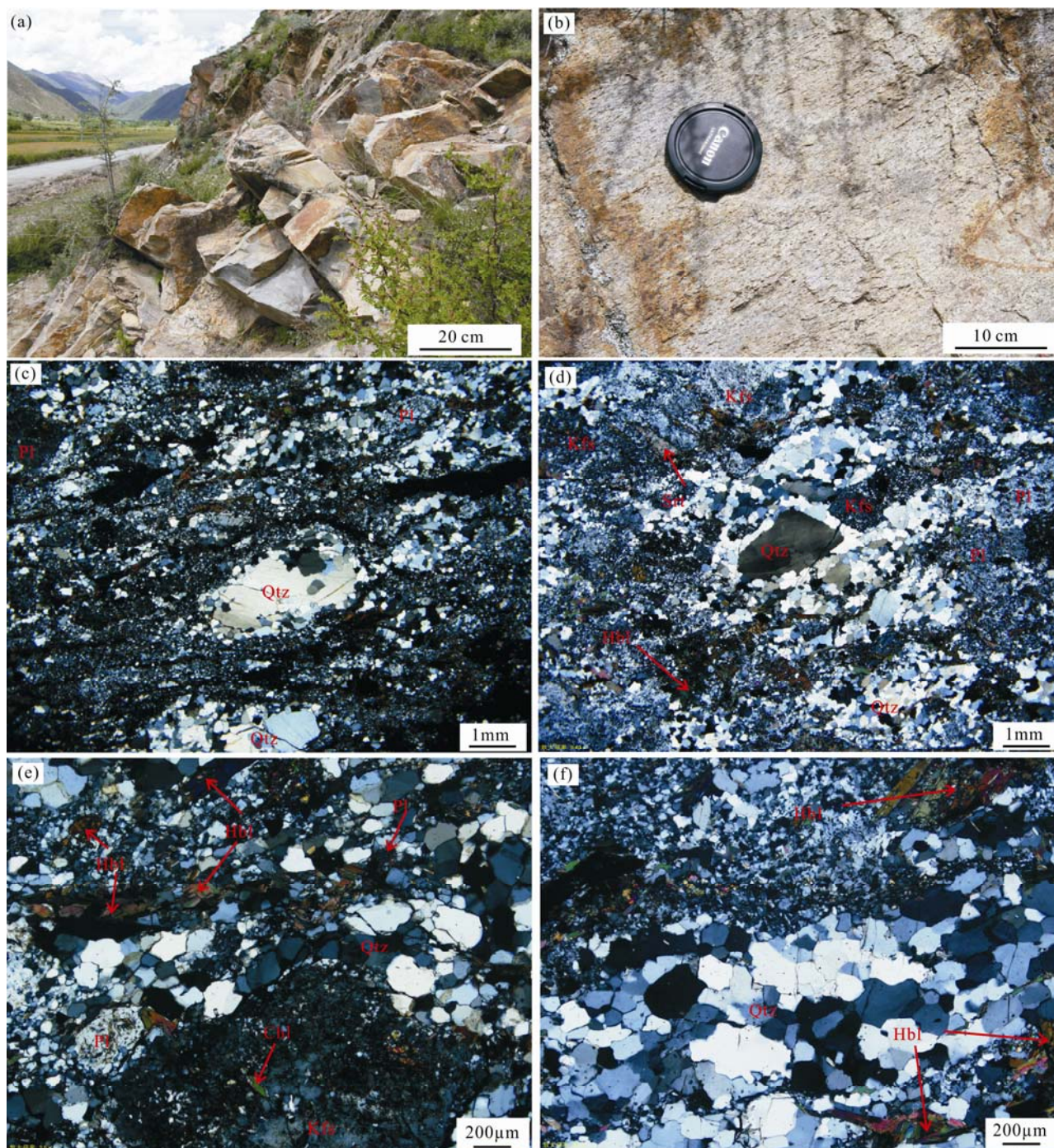


Fig. 2. Representative field photos and photomicrographs of the Daga mylonitic granite.
Pl=plagioclase; Qtz=quartz; Kfs=K-feldspar; Srt=sericite; Hbl=hornblende; Chl=chlorite.

crushed to 200-mesh mechanically, and then dried. The major elements were determined by X-ray fluorescence spectroscopy (XRF) and were detected by plasma spectroscopy and chemical method. Rare earth and trace elements were assayed using an ICP (PerkinElmer). The accuracy is better than 5%. The detailed procedures are described by Gao Jianfeng et al. (2003).

4 Results

4.1 Zircon U-Pb ages and Lu-Hf isotopes

Two representative samples from the mylonitic granite were dated using zircon LA-ICP-MS U-Pb methods and also selected for Lu-Hf isotope studies. The white line in Figure 3 represents U-Pb age domains and the red dotted line outlines different Lu-Hf isotopic domains,

respectively. On the cathode-luminescence images (Fig. 3), the analyzed zircon grains display euhedral crystal morphologies and oscillatory zoning, but no inherited zircons or metamorphic growth rims have been recorded. Some zircons contain small opaque inclusions. The analyzed zircons range in size from 50 μm to 160 μm , with length to width ratios ranging from 1:2 to 1:3. Based on the zircon morphologies and their high Th/U values (>0.4), these are considered as primary magmatic zircons (Hoskin and Schaltegger, 2003; Wu Yuanbao and Zheng Yongfei, 2004).

On the $^{207}\text{Pb}/^{235}\text{U}$ vs. $^{206}\text{Pb}/^{238}\text{U}$ concordia diagrams, all analytical points fall on the concordant curves, indicating no significant losses of Pb (Fig. 4). The crystallization ages of the Daga granite pluton, based on its zircon $^{206}\text{Pb}/^{238}\text{U}$ ratios, are about 225 ± 1.8 Ma (MSWD=0.30) and 229 ± 1.5 Ma (MSWD=0.51), respectively. These new

ages reveal another magmatic event at the beginning of Late Triassic in the Quxu region of southern Tibet. The detailed analytical results are listed in Table 2.

Zircon Lu-Hf isotope analyses were conducted parallel to the U-Pb domain dating (Fig. 3). Twenty zircon spots from the Daga pluton were analyzed for Lu-Hf isotopes. Five analyzes were neglected due to high uncertainties. The $^{176}\text{Hf}/^{177}\text{Hf}$ values vary from 0.283050 to 0.283092, $^{176}\text{Lu}/^{177}\text{Hf}$ values vary from 0.00191771 to 0.00315110, respectively. The $\varepsilon_{\text{Hf}}(t)$ values vary from +13.91 to +15.54, with a mean value of +14.79. The second model ages ($t_{\text{DM}2}$) range from 238 to 342 Ma, with a mean model age of 292 Ma. All results are listed in Table 3.

4.2 Whole-rock major and trace elemental geochemistry

Whole-rock major and trace element compositions are

Table 2 Zircon LA-ICP-MS isotopic data of the Daga granite pluton in the Quxu region, southern Tibet

Spot No.	Th	U	Th/U	$^{207}\text{Pb}/^{206}\text{Pb}$	1 σ	$^{207}\text{Pb}/^{235}\text{U}$	1 σ	$^{206}\text{Pb}/^{238}\text{U}$	1 σ	$^{208}\text{Pb}/^{232}\text{Th}$	1 σ	$^{207}\text{Pb}/^{235}\text{U}$	1 σ	$^{206}\text{Pb}/^{238}\text{U}$	1 σ	Concordance
XG1210-01	232	203	1.15	0.05184	0.00163	0.25163	0.00781	0.03522	0.00053	0.01158	0.00067	228	6	223	3	102
XG1210-02	125	111	1.13	0.05014	0.00435	0.25017	0.02080	0.03619	0.00103	0.01233	0.00164	227	17	229	6	99
XG1210-03	70	82	0.86	0.05046	0.00256	0.25012	0.01238	0.03597	0.00066	0.01335	0.00090	227	10	228	4	100
XG1210-04	147	154	0.95	0.05103	0.00193	0.24981	0.00930	0.03551	0.00059	0.01166	0.00073	226	8	225	4	101
XG1210-05	404	286	1.41	0.05155	0.00486	0.25117	0.02264	0.03533	0.00112	0.01153	0.00270	228	18	224	7	102
XG1210-06	32	49	0.64	0.05087	0.00641	0.24933	0.03027	0.03555	0.00133	0.01145	0.00205	226	25	225	8	100
XG1210-07	202	184	1.10	0.05128	0.00157	0.25063	0.00759	0.03545	0.00054	0.01231	0.00085	227	6	225	3	101
XG1210-08	139	160	0.86	0.05134	0.00261	0.25130	0.01244	0.03550	0.00072	0.01117	0.00107	228	10	225	4	101
XG1210-09	84	100	0.84	0.05138	0.00552	0.25094	0.02588	0.03543	0.00121	0.01460	0.00337	227	21	224	8	101
XG1210-10	37	63	0.58	0.05029	0.00414	0.25029	0.01990	0.03610	0.00095	0.01441	0.00213	227	16	229	6	99
XG1210-11	130	67	1.95	0.05041	0.00297	0.25102	0.01405	0.03612	0.00067	0.01183	0.00098	227	11	229	4	99
XG1210-12	215	90	2.38	0.05149	0.00247	0.24879	0.01128	0.03505	0.00055	0.01378	0.00120	226	9	222	3	102
XG1210-13	99	52	1.91	0.05071	0.00197	0.24945	0.00919	0.03568	0.00043	0.01021	0.00050	226	7	226	3	100
XG1210-14	46	30	1.55	0.05098	0.00631	0.24632	0.02923	0.03504	0.00127	0.01086	0.00200	224	24	222	8	101
XG1210-15	55	36	1.50	0.05072	0.00255	0.24926	0.01199	0.03565	0.00052	0.00942	0.00054	226	10	226	3	100
XG1210-16	64	32	2.02	0.04983	0.00309	0.24973	0.01480	0.03635	0.00066	0.00885	0.00057	226	12	230	4	98
XG1210-17	123	62	1.98	0.05027	0.01095	0.24468	0.05085	0.03530	0.00237	0.01002	0.00354	222	41	224	15	99
XG1210-18	53	34	1.57	0.05108	0.00780	0.25076	0.03672	0.03560	0.00159	0.01249	0.00299	227	30	226	10	101
XG1210-19	148	72	2.07	0.05087	0.00232	0.24783	0.01068	0.03534	0.00051	0.00710	0.00046	225	9	224	3	100
XG1210-20	74	41	1.80	0.05040	0.00459	0.24903	0.02168	0.03585	0.00098	0.01420	0.00275	226	18	227	6	99
XG1210-21	40	30	1.34	0.05111	0.00601	0.24626	0.02782	0.03496	0.00118	0.01117	0.00182	224	23	222	7	101
XG1210-22	60	45	1.33	0.05147	0.00589	0.24894	0.02723	0.03510	0.00120	0.01327	0.00250	226	22	222	8	101
XG1284-1	310	123	2.53	0.05098	0.00246	0.25598	0.01171	0.03642	0.00058	0.01181	0.00091	231	9	231	4	100
XG1284-2	193	78	2.47	0.05142	0.00221	0.25365	0.01029	0.03580	0.00049	0.01279	0.00094	230	8	227	3	101
XG1284-3	170	77	2.19	0.05052	0.00319	0.25910	0.01560	0.03720	0.00073	0.01197	0.00110	234	13	235	5	100
XG1284-4	153	73	2.10	0.05155	0.00357	0.26004	0.01718	0.03659	0.00079	0.01065	0.00094	235	14	232	5	101
XG1284-5	145	77	1.88	0.05015	0.01074	0.25416	0.05215	0.03670	0.00230	0.00723	0.00266	230	42	232	14	99
XG1284-6	63	37	1.74	0.05057	0.00400	0.25681	0.01947	0.03684	0.00085	0.01264	0.00124	232	16	233	5	100
XG1284-7	206	140	1.47	0.05110	0.00134	0.25367	0.00615	0.03601	0.00036	0.01164	0.00064	230	5	228	2	101
XG1284-8	172	89	1.93	0.05149	0.00481	0.25664	0.02285	0.03615	0.00105	0.01323	0.00213	232	18	229	7	101
XG1284-9	162	69	2.33	0.05179	0.00220	0.25798	0.01036	0.03613	0.00049	0.01209	0.00091	233	8	229	3	102
XG1284-10	201	107	1.89	0.05142	0.00688	0.25452	0.03246	0.03588	0.00151	0.00934	0.00218	230	26	227	9	101
XG1284-11	156	73	2.14	0.05129	0.00406	0.25435	0.01918	0.03598	0.00088	0.01403	0.00209	230	16	228	5	101
XG1284-12	118	67	1.76	0.05104	0.00327	0.25840	0.01576	0.03672	0.00074	0.01444	0.00174	233	13	232	5	100
XG1284-13	85	45	1.90	0.05062	0.00239	0.25827	0.01164	0.03701	0.00052	0.01335	0.00107	233	9	234	3	100
XG1284-14	61	43	1.41	0.05145	0.00284	0.25310	0.01334	0.03568	0.00056	0.01227	0.00120	229	11	226	3	101
XG1284-15	230	95	2.42	0.05075	0.00261	0.26051	0.01265	0.03725	0.00061	0.01353	0.00171	235	10	236	4	100
XG1284-16	320	115	2.77	0.05111	0.00194	0.25286	0.00902	0.03588	0.00047	0.01234	0.00081	229	7	227	3	101
XG1284-17	184	95	1.93	0.05149	0.00408	0.25587	0.01928	0.03600	0.00089	0.01247	0.00208	231	16	228	6	101
XG1284-18	333	124	2.68	0.05123	0.00205	0.25540	0.00962	0.03616	0.00049	0.01298	0.00102	231	8	229	3	101
XG1284-19	121	60	2.03	0.05120	0.00326	0.25721	0.01560	0.03644	0.00072	0.01292	0.00127	232	13	231	4	100
XG1284-20	162	88	1.85	0.05156	0.00364	0.25941	0.01740	0.03651	0.00081	0.01229	0.00178	234	14	231	5	101
XG1284-21	110	67	1.65	0.05083	0.00297	0.25602	0.01425	0.03654	0.00066	0.01260	0.00130	231	12	231	4	100
XG1284-22	70	48	1.45	0.05134	0.00459	0.25782	0.02205	0.03642	0.00098	0.01097	0.00163	233	18	231	6	101
XG1284-23	128	70	1.84	0.05088	0.00381	0.25671	0.01837	0.03660	0.00084	0.01455	0.00202	232	15	232	5	100
XG1284-24	187	88	2.12	0.05090	0.00300	0.25807	0.01446	0.03678	0.00069	0.01271	0.00150	233	12	233	4	100
XG1284-25	136	57	2.38	0.05155	0.00521	0.25995	0.02508	0.03657	0.00113	0.01521	0.00305	235	20	232	7	101

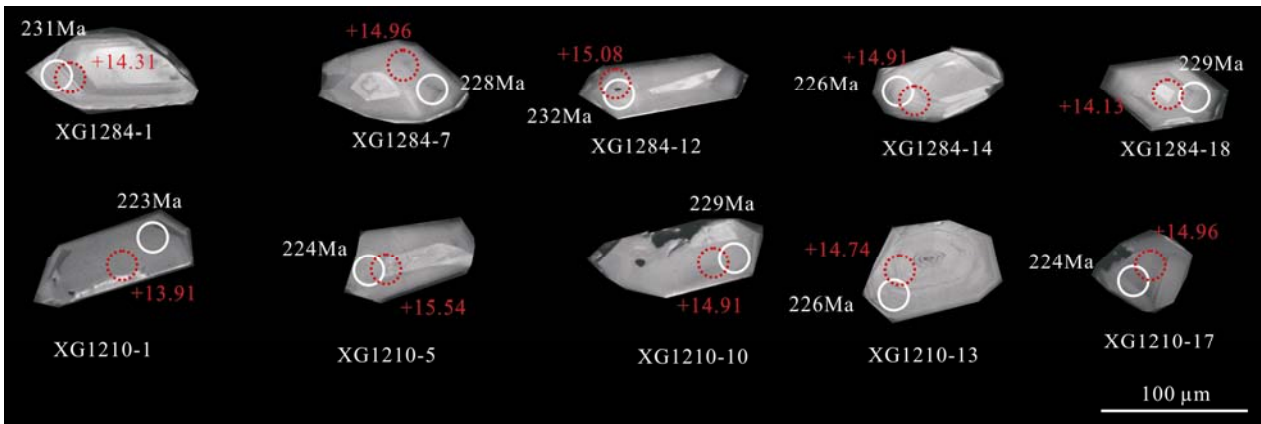


Fig. 3. Representative CL images of zircons from the Daga granite, white circle for U-Pb dating domains, and red dotted circle for Lu-Hf analysis domains.

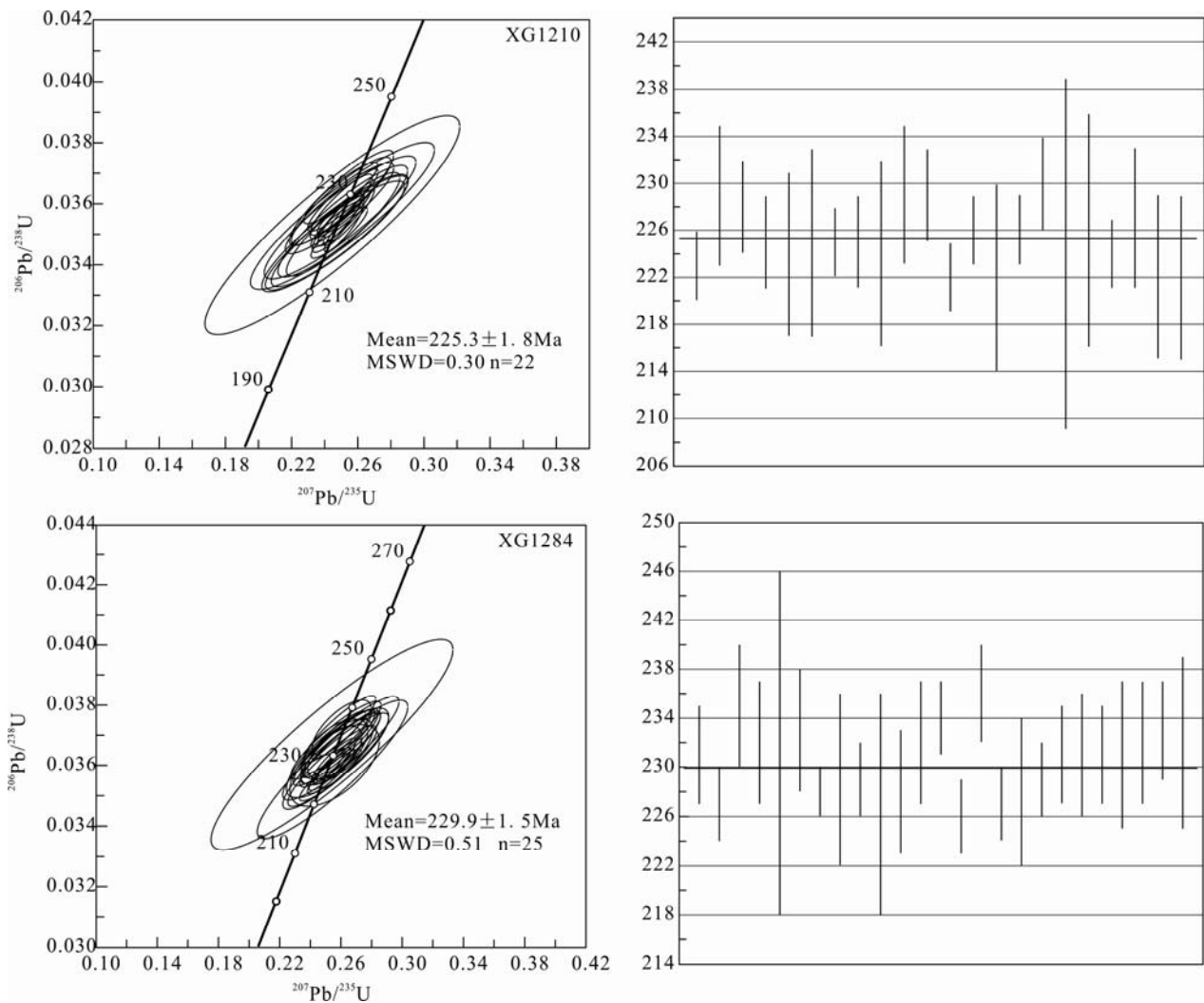


Fig. 4. Zircon LA-ICP-MS U-Pb concordia diagrams of the Daga granite from the Quxu batholith in the middle Gangdese belt, southern Tibet.

presented in Table 4. The Daga granitic pluton has variable SiO_2 contents ranging from 67.5 to 71.92 wt% and low $\text{K}_2\text{O}+\text{Na}_2\text{O}$ contents ranging from 4.41 to 5.86 wt%, respectively. The Rittmann Index δ ranges from 0.73

to 1.34 (mean $\delta=1.00<3.3$), indicating a calc-alkaline rock affinity [$\delta=(\text{Na}_2\text{O}+\text{K}_2\text{O})^2/(\text{SiO}_2-43)$]. The analyzed samples have low LOI between 0.72 and 1.14 (mean 0.85) (Table 4), confirming that the Daga granite is largely

Table 3 Representative zircon Lu–Hf isotope data of the Daga granite pluton in the Quxu region, southern Tibet

Spot No.	<i>t</i> (Ma)	¹⁷⁶ Yb/ ¹⁷⁷ Hf	¹⁷⁶ Lu/ ¹⁷⁷ Hf	2σ	¹⁷⁶ Hf/ ¹⁷⁷ Hf	2σ	<i>ε</i> _{Hf} (<i>t</i>)	2σ	<i>T</i> _{DM1}	2σ	<i>T</i> _{DM2}
XG1210-01	225	0.129031	0.003151	0.000018	0.28305	0.000025	13.91	0.89	303	38	342
XG1210-05	225	0.084295	0.002096	0.000039	0.283092	0.000021	15.54	0.73	233	30	238
XG1210-10	225	0.088086	0.002217	0.000043	0.283074	0.000019	14.91	0.68	260	28	278
XG1210-13	225	0.114446	0.002879	0.000012	0.283072	0.000025	14.74	0.88	267	37	289
XG1210-15	225	0.103566	0.002522	0.000103	0.28307	0.000021	14.71	0.73	268	31	291
XG1210-17	225	0.082678	0.002158	0.000065	0.283075	0.000021	14.96	0.73	257	30	275
XG1210-23	225	0.081922	0.002204	0.000027	0.283067	0.000022	14.67	0.78	269	33	293
XG1284-01	230	0.108209	0.002799	0.000031	0.283057	0.000021	14.31	0.75	289	32	320
XG1284-06	230	0.074303	0.001936	0.000059	0.283078	0.000019	15.17	0.67	252	28	265
XG1284-07	230	0.095851	0.002463	0.000072	0.283063	0.000026	14.96	0.94	279	39	305
XG1284-08	230	0.075354	0.001934	0.000015	0.283071	0.000019	14.93	0.68	263	28	281
XG1284-12	230	0.078451	0.00202	0.000016	0.283075	0.000019	15.08	0.69	256	29	271
XG1284-14	230	0.076946	0.001918	0.000028	0.283059	0.00002	14.91	0.7	280	29	308
XG1284-18	230	0.141708	0.003406	0.000106	0.283055	0.000023	14.13	0.82	298	35	332
XG1284-19	230	0.076606	0.001934	0.000029	0.283069	0.00002	14.86	0.7	266	29	285

Table 4 Major (wt%) and trace (ppm) element compositions of the Daga pluton in the Quxu region, southern Tibet

Items/Sample No.	XG1284-01	XG1284-02	XG1284-03	XG1284-04	XG1210-01	XG1210-02	XG1210-03
SiO ₂	70.10	68.71	67.50	69.48	71.82	70.21	71.92
TiO ₂	0.43	0.42	0.40	0.38	0.37	0.37	0.34
Al ₂ O ₃	14.05	14.47	14.84	13.79	13.86	14.20	13.77
Fe ₂ O ₃ ^T	4.36	4.31	4.56	3.99	3.65	4.18	3.43
FeO ^T	3.92	3.88	4.10	3.59	3.29	3.76	3.09
MnO	0.08	0.09	0.12	0.11	0.09	0.07	0.10
MgO	1.96	1.88	1.93	1.38	1.52	1.84	1.24
CaO	3.37	3.83	3.11	4.93	2.54	3.45	3.10
Na ₂ O	3.75	3.87	4.33	3.53	4.46	3.93	4.22
K ₂ O	1.37	1.34	1.40	0.88	1.16	1.10	0.91
P ₂ O ₅	0.09	0.10	0.08	0.09	0.08	0.08	0.07
LOI	0.75	0.92	0.92	1.14	0.7	0.79	0.7
Total	100.31	99.94	99.19	99.70	100.25	100.22	99.80
Trace and REE elements							
Ti	2580	2520	2400	2280	2220	2220	2040
Rb	17.7	15.3	15.2	10.4	12.6	16.0	10.2
Ba	242	203	233	166	235	198	166
Th	2.19	1.57	2.28	1.49	2.39	3.00	2.55
U	0.56	0.36	0.81	0.34	0.78	0.73	0.83
Nb	1.40	1.30	1.60	1.20	1.50	1.60	1.50
Ta	0.20	0.10	0.10	0.10	0.10	0.10	0.10
Sr	235	289	284	345	232	234	281
Nd	15.40	12.40	16.80	13.10	15.20	14.40	15.10
Sm	3.40	3.09	4.23	3.11	3.64	3.16	3.50
Zr	140	124	145	119	143	154	120
Hf	3.70	3.10	3.90	3.20	4.00	4.40	3.40
Tb	0.57	0.50	0.65	0.51	0.51	0.51	0.53
Y	19.40	18.20	23.70	17.20	19.60	18.30	18.10
Yb	2.27	1.93	2.63	1.87	2.26	2.16	2.03
Lu	0.36	0.31	0.42	0.31	0.37	0.36	0.32
La	12.10	8.80	11.90	10.00	11.20	12.40	12.20
Ce	28.20	20.90	28.40	23.00	26.50	26.70	27.60
Pr	3.38	2.64	3.54	2.87	3.29	3.14	3.37
Eu	0.88	0.82	0.96	0.79	0.77	0.78	0.77
Gd	3.71	3.42	4.19	3.17	3.49	3.12	3.18
Dy	3.22	3.05	4.04	2.97	3.18	2.95	3.11
Ho	0.70	0.64	0.83	0.61	0.67	0.62	0.67
Er	2.20	1.97	2.59	1.85	2.23	2.05	2.08
Tm	0.33	0.30	0.41	0.28	0.33	0.33	0.31
K ₂ O+Na ₂ O	5.12	5.21	5.73	4.41	5.62	5.03	5.13
δ	0.97	1.06	1.34	0.73	1.10	0.93	0.91
Mg [#]	49.98	49.22	48.47	43.46	48.07	49.45	44.55
A/NK	1.84	1.85	1.72	2.04	1.61	1.85	1.74
A/CNK	1.02	0.98	1.04	0.88	1.05	1.02	1.01
Eu/ [*] Eu	0.76	0.77	0.70	0.77	0.66	0.76	0.71
Ti/Zr	18.43	20.32	16.55	19.16	15.52	14.42	17.00
Rb/Sr	0.08	0.05	0.05	0.03	0.05	0.07	0.04
Y+Nb	20.80	19.50	25.30	18.40	21.10	19.90	19.60
Th/Ta	10.95	15.70	22.80	14.90	23.90	30.00	25.50
LREE/HREE	6.95	5.99	6.05	6.67	6.71	7.09	7.26
(La/Yb) _N	3.83	3.27	3.25	3.84	3.56	4.12	4.31

unaffected by hydrothermal alteration, as previously documented in petrographic thin sections.

On the SiO_2 vs. $\text{Na}_2\text{O}+\text{K}_2\text{O}$ (TAS) diagram (Fig. 5a), all the samples plot in the granodiorite field, with sub-alkaline compositions (SA), consistent with thin sections observations (Fig. 2c–f). On the SiO_2 vs. K_2O diagram, the samples fall into the low-K to middle K calc-alkaline series (Fig. 5b). Besides, the A/CNK (molar $\text{Al}_2\text{O}_3/\text{CaO}+\text{K}_2\text{O}$) ratios of the samples vary between 0.88 and 1.05 (mean value of 1.0), showing a metaluminous I-type granitic signature (Fig. 5c). As shown on the SiO_2 vs. $\text{Mg}^\#$ diagram (Fig. 5d), the Daga granite has average $\text{Mg}^\#$ numbers of 47.61, which is higher than that of typical crustal melts and suggests some mantle input during its genesis (Rapp and Watson, 1995).

The Daga granite has moderate enrichments of light rare earth elements (LREE) in comparison to the heavy rare earth elements (HREE) (LREE/HREE ratios varying from 2.05 to 2.41; $[\text{La}/\text{Yb}]_N=3.05-4.05>1$) (Fig. 6a), and shows subtle negative Eu anomalies in their REE patterns ($\text{Eu}/$

* $\text{Eu}=0.66-0.77$, mean value=0.73), suggestive plagioclase fractionation during their magma evolution. Additionally, the samples are characterized by enrichments of incompatible elements and LILE, such as Rb, Ba, Th, U, and pronounced depletions of high field elements (HFSE), such as Nb, Ta, Ti, P (Fig. 6b). Those trace element signatures typically require partial melting of an enriched subduction-arc setting (Fig. 6) (Saunders et al., 1980; Kelemen et al., 1990).

5 Discussion

5.1 Zircon genesis and emplacement age

Late Triassic magmatic activities in the Gangdese belt were documented (Chu et al., 2006; He Zhonghua et al., 2005, 2006; Ji et al., 2009; Ji Weiqiang et al., 2009; Zhu et al., 2011; Peng Jianhua et al., 2013; Song Shaowei et al., 2014; Meng et al., 2016a, b; Wang et al., 2016; Ma et al., 2017). In the study area, a Late Triassic hornblende gabbro pluton was recognized by Meng et al. (2016a) (Fig.

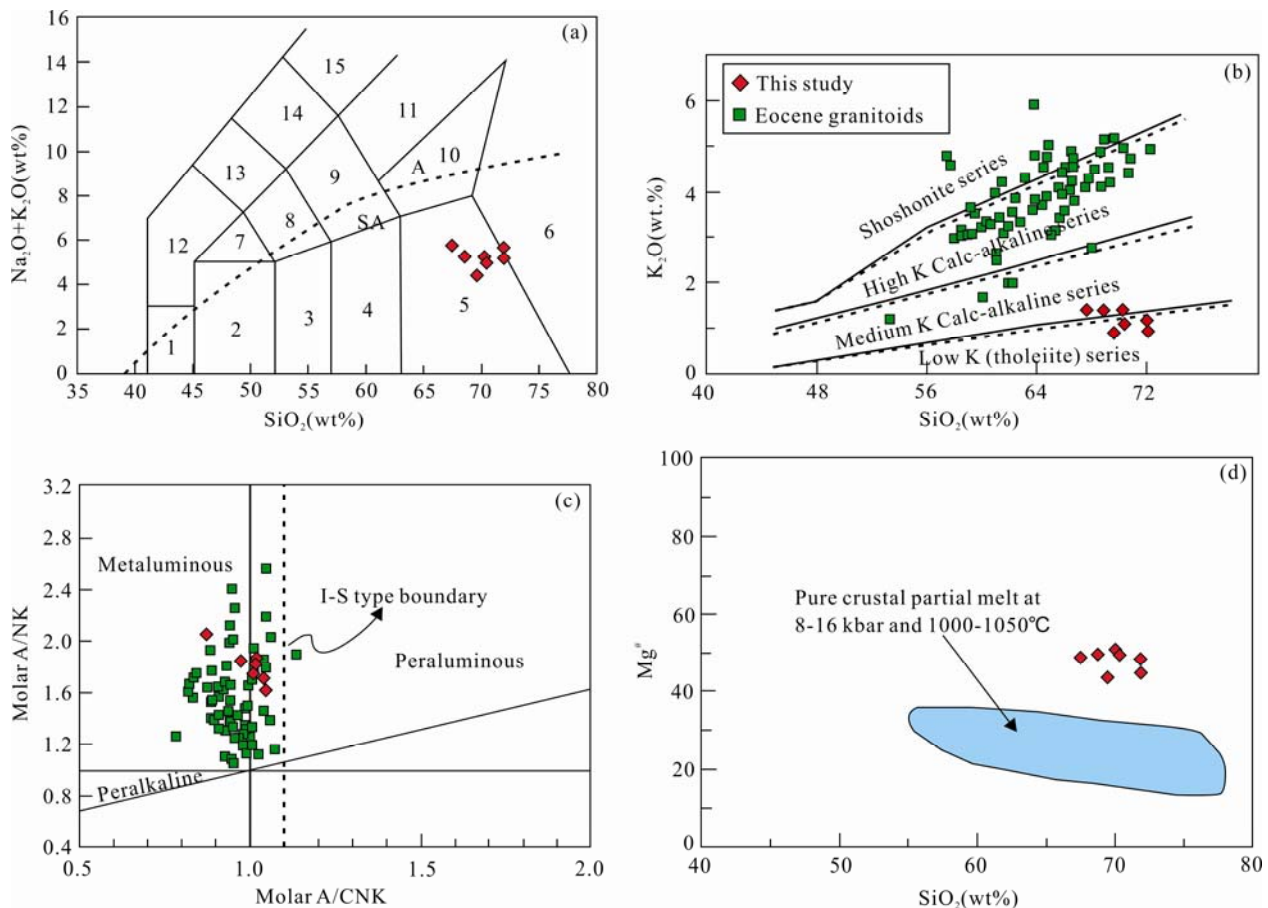


Fig. 5. (a), TAS diagram (after Peccerillo and Taylor, 1976; Middlemost, 1994). (b), SiO_2 vs. K_2O discrimination diagram and (c), Molar A/CNK vs. Molar A/NK diagram (after Maniar and Piccoli, 1989); (d), SiO_2 vs. $\text{Mg}^\#$ diagram ($\text{Mg}^\# = \text{Mg}/(\text{Mg} + \text{Fe}^{\text{T}})$) (Rapp and Watson, 1995) (Eocene granitoids of the Quxu batholith are referred to Chen Tao, 2006, Xu Wangchun, 2010 and Ma et al., 2016).

A=alkaline; SA=sub-alkaline; 1=peridotgabbro; 2=sub-alkaline gabbro; 3=gabbro diorite; 4=diorite; 5=granodiorite; 6=granite; 7=quartzite; 8=alkaline gabbro; 9=monzogabbro; 10=monzodiorite; 11=monzonite; 12=adamellite; 13=syenite; 14=foiid gabbro; 15=foiid monzodiorite; 16=foiid monzosyenite; 17=foiid syenite; 18=foiidolite.

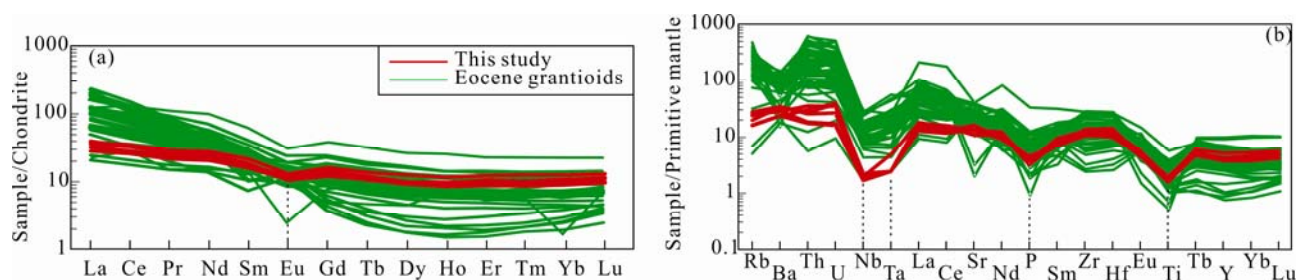


Fig. 6. (a), Chondrite-normalized REE patterns; (b), Primitive mantle-normalized multiple trace element diagram.

The Chondrite values are from Boynton (1984), and the primitive mantle values are from Sun and McDonough (1989) (Eocene granitoids of the Quxu batholith are referred to Chen Tao, 2006, Xu Wangchun, 2010 and Ma et al., 2016).

1c). Since, it is widely accepted that the Quxu batholith is dominantly composed of Eocene granitoid rocks (Chen Tao, 2006; Ji et al., 2009; Mo Xuanxue et al., 2009; Xu Wangchun, 2010; Ma et al., 2016), it is essential to discriminate the zircon sources and genesis, with the aim of better understanding the evolution of the Daga granitic pluton. Generally speaking, inherited zircons are mainly derived from overlying sediments, basement rocks or adjacent intrusions. According to the zircons morphology, and age distribution, we can discriminate inherited zircons from primary magmatic zircons. For example, basic stocks or dykes can easily collect inherited zircons when they pass through a granitic batholith. Those zircons captured by the basic rocks or dykes typically show oscillatory zoning. If the magma passes through sedimentary rocks, the inherited zircons will reveal different age distributions. Furthermore, the inherited zircons from the sedimentary rocks typically contain cracks, and do not have idiomorphic shapes as well as a poor transparency compared with primary magmatic zircons (Chen Tao, 2006). In this paper, zircons from the Daga pluton show typical euhedral shapes and oscillatory zoning indicative of magmatic growth. Compared with the nearly contemporaneous basic intrusive pluton (Fig. 1b–c), the analyzed zircons differ from basic zircon morphology in showing broad zoning and banded textures. Taking into account the temporal and spatial distribution of the Late Triassic igneous rocks and zircon morphology, we conclude that the studied zircons are primary magmatic zircons from the Daga granitic pluton. Zircon U–Pb dating results reveal that two samples from different parts of the Daga pluton provide weighted ages of 225.3 ± 1.8 Ma and 229.9 ± 1.5 Ma, respectively. Those weighted mean ages are indistinguishable within the analytical error bars and are interpreted as the crystallization age of the Daga granitic pluton.

Recently, Ma et al. (2016) reported Triassic inherited zircons in the Eocene Quxu batholith. This suggests that the Eocene Quxu batholith could have assimilated Late Triassic intrusions.

5.2 Petrogenesis

Granites can form in different tectonic settings (Condie, 1982; Pearce et al., 1984; Chappell et al., 1998; Barbarin, 1990, 1999; Winter, 2001; Xu Xisheng and Qiu Jiansheng, 2010; Wang Tao et al., 2017). Hence, granitic rocks are the key in evaluating the geodynamic setting of tectonic terranes (Barbarin, 1990; Winter, 2001; Wang Tao et al., 2017). It is generally assumed that hornblende-bearing granites with calc-alkaline compositions and I-type affinities are the evolved products of subduction arcs. By contrast, cordierite-bearing, two-mica granites are considered as products of the melting of Al-rich sediments (S-type). Potassic calc-alkaline granites are commonly found in post-collisional settings. Additionally, alkaline and peralkaline granites (A-type) are usually related to rifting and continental uplift in within-plate settings. M-type granites, the evolved products of mafic sources show similar geochemical signatures with mafic rocks as indicated by enrichments of Cr, Co, Mg, Ni and V elements (Xu Xisheng and Qiu Jiansheng, 2010; Cen Kuang and Chen Yuan, 2011). These different granitic types enable us to effectively evaluate their regional tectonic settings and magma sources (Barbarin, 1990; Winter, 2001; Cen Kuang and Chen Yuan, 2011; Wang Tao et al., 2017). The studied samples from the Daga pluton show I-type signatures ($A/CNK < 1.1$) with hornblende-bearing low-K calc-alkaline compositions (Fig. 5b–c). Besides, the effective discrimination diagrams also suggest I-type granitic trends (Fig. 7a–b). As discussed above, we propose that the Daga pluton might be products of the northward subduction of the Neo-Tethys Ocean.

Experimental petrology reveals that granitic rocks can be formed by partial melting of different protoliths during a relatively wide range of temperature and pressure conditions (Rapp et al., 1991, 1995; Wolf and Wyllie, 1994; Patino Douce and Beard, 1996; Winter, 1996; Patino Douce and McCarthy, 1998; Skjerlie and Douce, 2002). In general, geochemical fingerprints of the melts mainly depend on their parental materials, as well as on

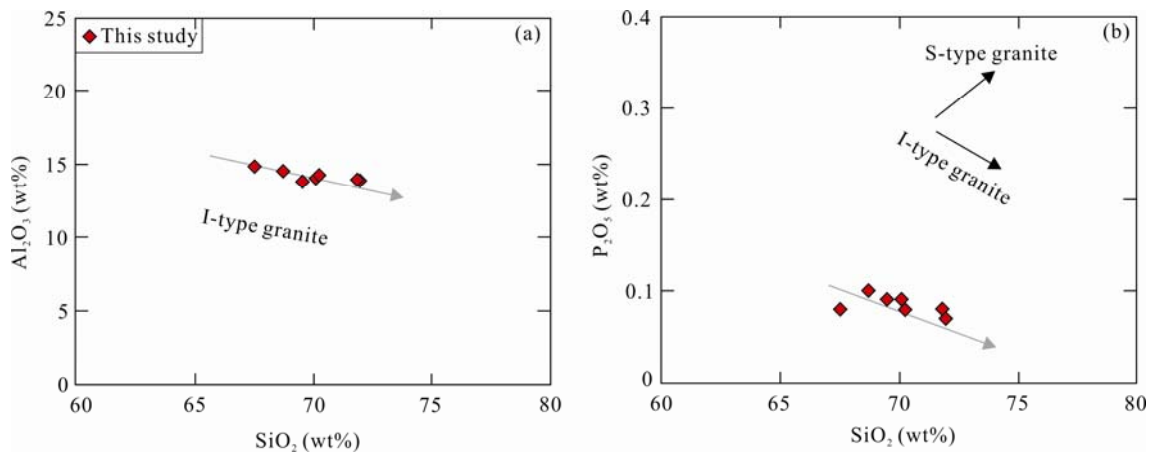


Fig. 7. (a) Al_2O_3 vs. SiO_2 and (b) SiO_2 vs. P_2O_5 plots (after Chappell, 1999).

the temperature and pressure conditions and their water contents during partial melting (Jogvan et al., 2006; Xu Xisheng and Qiu Jiansheng, 2010). For example, partial melting of mudstones usually results in Al-rich and K-rich granitic melts; the partial melting of greywackes can generate moderately Al-rich and K-rich granodioritic or granitic melts; the partial melting of meta-basaltic rocks commonly produce trondhjemite-granodiorite melts (Rapp et al., 1991, 1995; Winther, 1996). In summary, calc-alkaline granitic melts form where volatile phases such as water are present (Patino Douce, 1999). The discrimination diagrams show that the Daga granitic pluton falls into the amphibolite and meta-basaltic fields, indicating that the granite pluton was derived from the partial melting of lower crustal material (Fig. 8a–b). Notably, the Lu-Hf isotope data indicate that the samples are characterized by highly positive $\varepsilon_{\text{Hf}}(t)$ values adjacent to the depleted mantle line (Fig. 9a, c) and young second model ages (Fig. 9d), suggesting that their protoliths were

formed by partial melting of juvenile crust (Wu Fuyuan et al., 2007). The juvenile crust mainly is originated from basaltic magmas derived from the depleted mantle. Their emplacement caused the partial melting of, and assimilation with, juvenile crustal material, and hence, generating the Late Triassic magmatic products. Note that all the samples show high $\text{Mg}^\#$ values (over 40) (Fig. 5d) suggesting the participation of mantle components consistent with Hf isotopic compositions. Therefore, magma mixing was probably involved in the evolution of the Daga pluton. Importantly, the studied samples plot on the lines of magma mixing (Fig. 10a–b). Based on discrimination diagrams and the spatial distribution of coeval mafic rocks (Meng et al., 2016a; Wang et al., 2016) (Fig. 1b–c), the basaltic magma could represent the mafic end member, then felsic end member being acidic magma derived from crustal material. Qiu Jiansheng et al. (2015) point out that multiple underplating of mafic magmas and induced magma mixing probably occurred during the

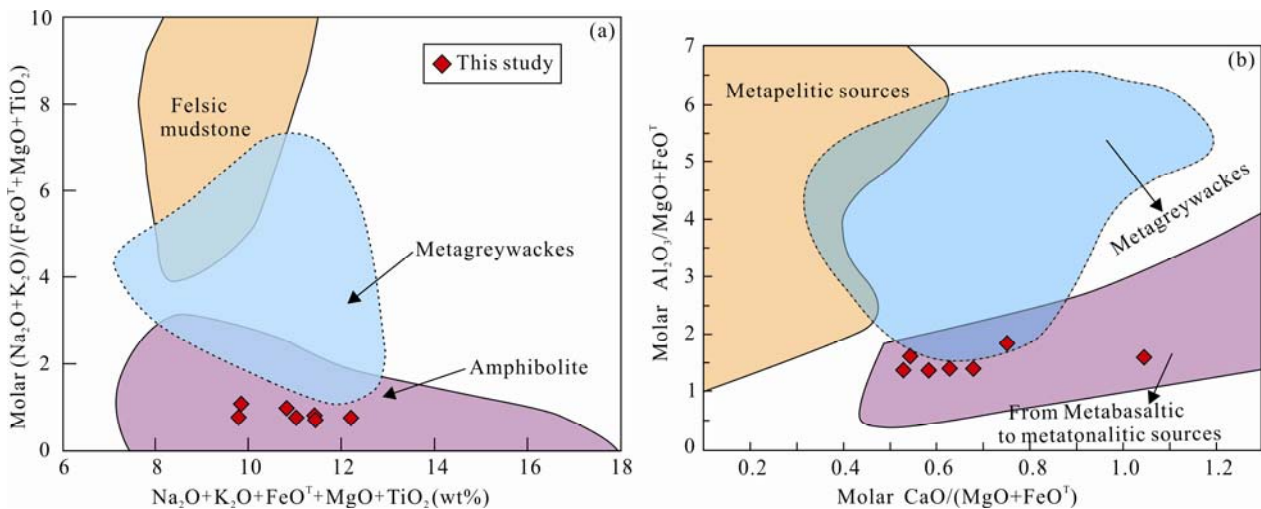


Fig. 8. (a), $(\text{Na}_2\text{O}+\text{K}_2\text{O}+\text{FeO}^{\text{T}}+\text{MgO}+\text{TiO}_2)$ vs. $(\text{Na}_2\text{O}+\text{K}_2\text{O}/\text{FeO}^{\text{T}}+\text{MgO}+\text{TiO}_2)$ discrimination diagram for the Daga pluton (after Patino Douce, 1999); (b), Molar $\text{Al}_2\text{O}_3/(\text{MgO}+\text{Fe}_2\text{O}_3^{\text{T}})$ vs. molar $\text{CaO}/(\text{MgO}+\text{Fe}_2\text{O}_3^{\text{T}})$ diagram, showing the source composition for the Daga granite (after Altherr et al., 2000).

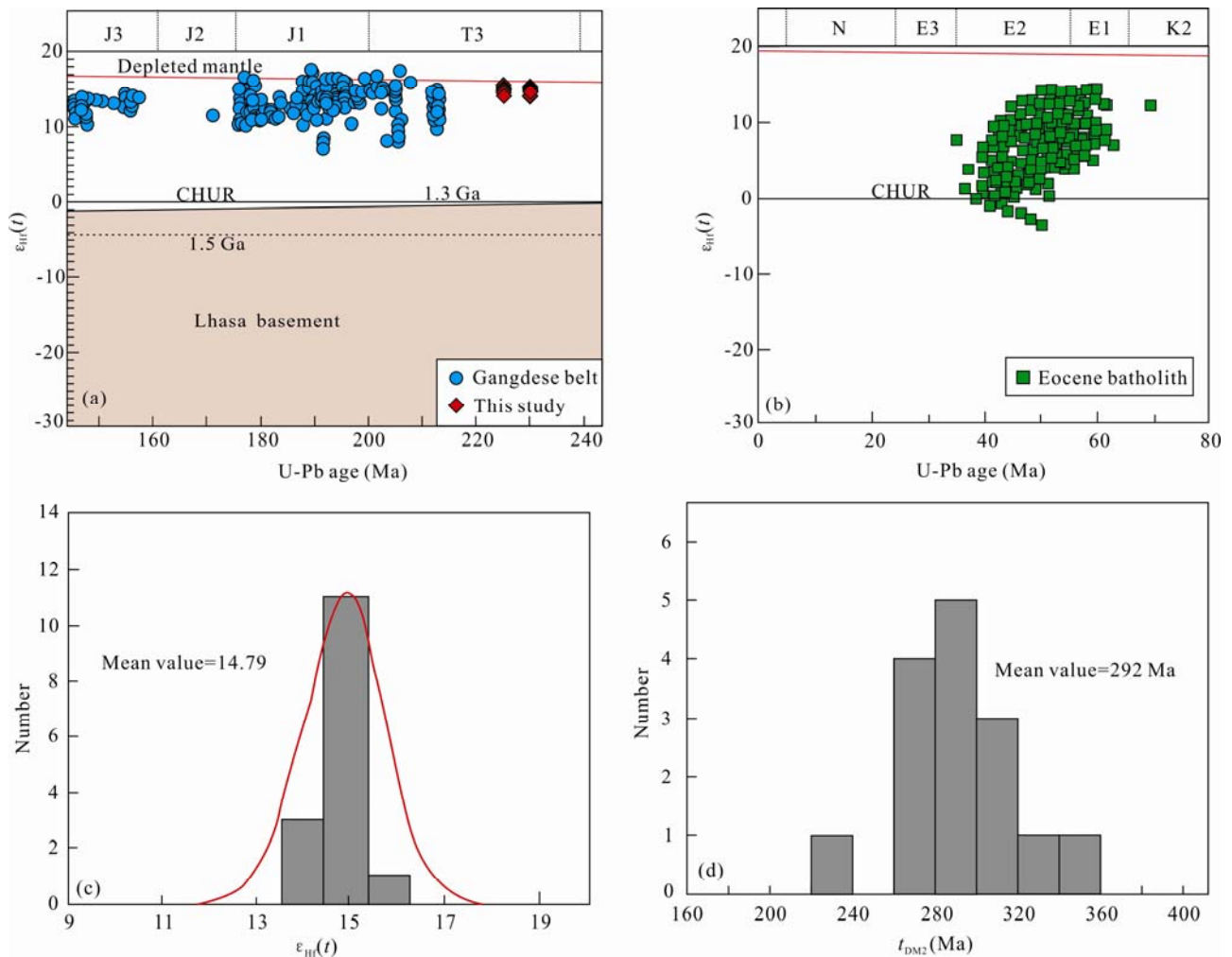


Fig. 9. (a), Zircon $\varepsilon_{\text{Hf}}(t)$ values vs. U-Pb ages (Ma) variations (Referred data from Zhang Hongfei et al., 2007; Ji Weiqiang et al., 2009; Meng et al., 2016a, b; Ma et al., 2017); (b) zircon $\varepsilon_{\text{Hf}}(t)$ values vs. U-Pb ages of the Quxu granitoid batholith (after Ji et al., 2009; Xu Wangchun, 2010; Ma et al., 2016); (c-d) the histograms of $\varepsilon_{\text{Hf}}(t)$ values and t_{DM2} (second model) ages.

entire duration (>205–40 Ma) of the Neo-Tethys Ocean. This geodynamic process is common in subduction arc settings (Foley and Wheller, 1990; Anthony, 2005).

5.3 Comparison with the Quxu Eocene granitic batholith

The Quxu batholith is mainly composed of diorites, granodiorites, monzogranites, quartz diorites, and rare mafic intrusions. Zircon U-Pb dating results demonstrate that the Quxu composite batholith formed during the Paleocene to Eocene (60–41 Ma) (Ji Weiqiang et al., 2009; Mo Xuanxue et al., 2009). Eocene granitoids are the major components of the Quxu composite batholith and they were dated at ca. 47–52.5 Ma (Dong Guochen et al., 2005; Mo Xuanxue et al., 2005a, b, 2009; Chen Tao, 2006; Wen et al., 2008; Ji et al., 2009; Xu Wangchun, 2010), which is consistent with the diagenetic ages of the Linzizong volcanic units. Previous studies reveal that the Quxu composite batholith has a high K calc-alkaline

composition which is different to the Late Triassic granitic rocks considered in this study (Fig. 5b). On the A/CNK vs. A/NK diagram (Fig. 5c), the granitoid samples from the Quxu batholith also reveal I-type granite affinities. Similar to the Late Triassic Daga granite pluton, the samples from the Quxu batholith are also characterized by high $\text{Mg}^\#$ values, which are probably related to basaltic magma underplating during the Eocene. Dong et al. (2005) and Mo et al. (2005b) note that the Quxu composite batholith formed from mixing between felsic and mafic magmas. Additionally, the large variation in $\varepsilon_{\text{Hf}}(t)$ values reflects Hf isotopic heterogeneity in the magma sources of the Quxu batholith. By contrast, the Late Triassic granitic rocks have small variations in $\varepsilon_{\text{Hf}}(t)$ values suggesting that they were derived from depleted mantle sources (Fig. 9a). In conclusion, the Daga granite pluton and the Eocene batholith in the Quxu region have similar REE patterns and spider diagrams (Fig. 6) characterized by arc-related geochemical affinities; however, the Daga granite pluton

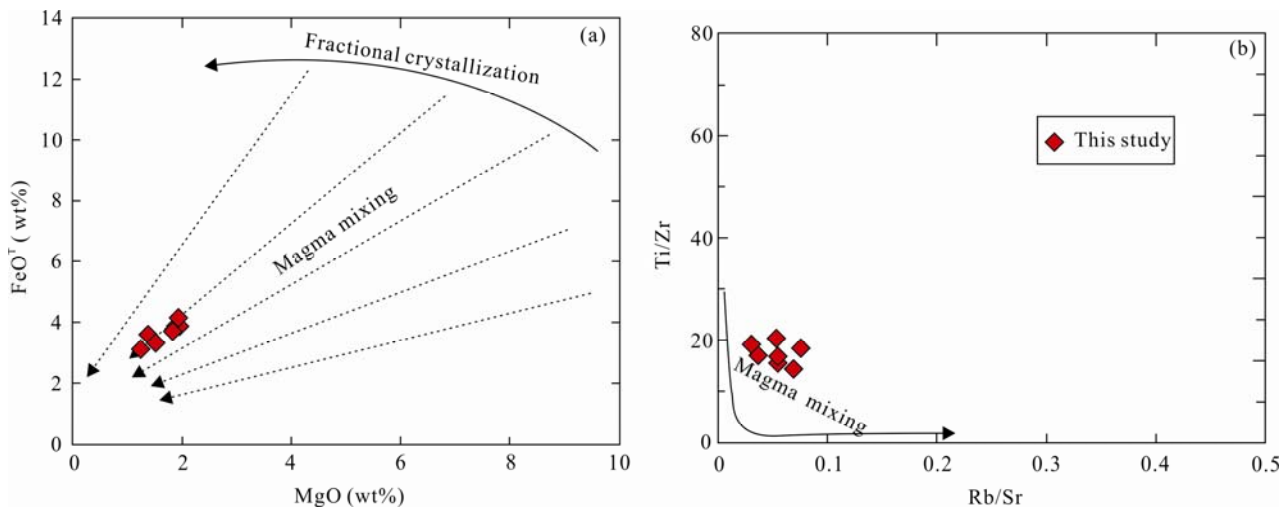


Fig. 10. (a), Diagram of FeO^T vs. MgO (after Zorpi et al., 1991); (b), Ti/Zr vs. Rb/Sr diagram (de Hollanda et al., 2003).

shows different major elements geochemical signatures and Hf isotopic components (Fig. 5, Fig. 9) suggesting different petrogenesis and tectonic scenario.

5.4 Tectonic implications

It is widely accepted that the Cretaceous magmatism in southern Tibet was closely related to the northward subduction of the Neo-Tethys paleo-ocean. However, the pre-Cretaceous tectonic setting is still under debate (Geng Quanru et al., 2006; Zhang Hongfei et al., 2007; Ji et al., 2009; Ji Weiqiang et al., 2009; Zhu et al., 2011; Dong Xin and Zhang Zeming, 2013; Wang Cheng et al., 2014; Meng et al., 2016a, b; Ma et al., 2017). In this study, the mylonitic granite from the Quxu batholith shows highly positive $\varepsilon_{\text{Hf}}(t)$ values and relatively young model ages, enriched LREE and LILE and depleted HFSE with negative Nb, Ta and Ti anomalies, all of which suggest a continental arc-related setting (Perfit et al., 1980). Moreover, positive Ce anomalies in mantle-normalized REE patterns also indicate that the Daga pluton formed in a subduction arc setting (Fig. 6a) (Perfit et al., 1980).

In general, the Yb vs. Ta and Rb vs. (Y+Nb) diagrams are effective in discriminating the tectonic setting of granitoids. The samples from the Daga pluton plot in the volcanic arc field (Fig. 11a–b). This is also consistent with the Y vs. Zr discrimination diagram (Fig. 11c). A subduction-related tectonic setting is also suggested by the Yb vs. Th/Ta discrimination diagram (Pearce and Peate, 1995). Using ratios and relative abundances of incompatible elements, Gorton and Schandl (2000) were able to discriminate between oceanic arcs, continental arcs and within-plate tectonic settings based on a geochemical dataset of granites from 26 different locations. Gorton and Schandl (2000) divide the Th/Ta ratios into three intervals, 1–6 for within-plate magmatism, 6–20 for continental arcs

and >20 for oceanic arcs. The samples from the Daga pluton have Th/Ta ratios of >6, suggesting a continental arc setting (Fig. 11c). Consistent with previous studies (He Zhonghua et al., 2005, 2006; Ji et al., 2009; Kang et al., 2014; Meng et al., 2016a, b; Ma et al., 2017), our data confirm that the northward subduction of the Neo-Tethys oceanic crust occurred no later than the Late Triassic (Carnian stage). Our data demonstrates that southern Tibet developed from an active continental margin, implying that the Neo-Tethys Ocean has experienced a long evolutionary history extending over 170 Ma.

In the Gangdese belt, other igneous rocks also suggest that the Neo-Tethys Ocean developed over a long history, and that the subduction commenced in the Late Triassic. He Zhonghua et al. (2005, 2006) report Late Triassic granite in the Menba region, southern Tibet, and consider the granite to be the products of the Neo-Tethys oceanic northward subduction. These authors suggest that the Gangdese magmatic belt formed as early as Late Triassic. Additionally, a Late Triassic (205 Ma) foliated granite recorded in the Dazhuka region by Ji et al. (2009) is exposed in the vicinity of the IYTSZ. In accordance with He Zhonghua et al. (2005, 2006) and Chu et al. (2006), Ji et al. (2009) suggest that the northward subduction of the Neo-Tethys probably commenced during Late Triassic, at least prior to 205 Ma, and continued until Late Paleocene. Therefore, both the ~210 Ma mylonitic granite and the 210–212 Ma hornblende gabbro documented near the Kazi township in Namling county and in the Qinxu region of Quxu county, respectively, provide the petrological key to understand the tectonic framework of southern Tibet (Meng et al., 2016a; Ma et al., 2017). Meng et al. (2016a) suggest that the Late Triassic mylonitic granite and the hornblende gabbro are products of the northward subduction of the Neo-Tethys paleo-ocean. Ma et al.

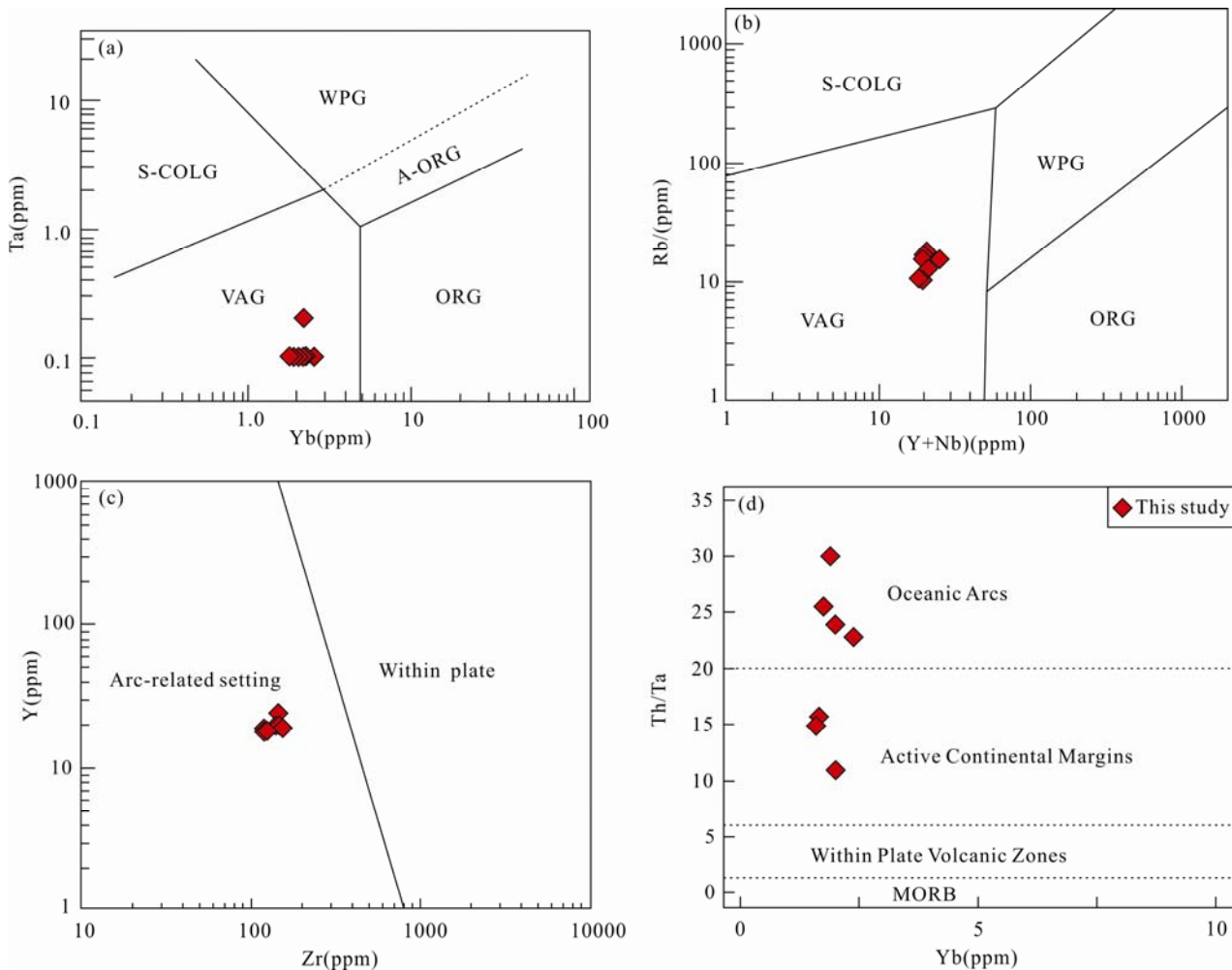


Fig. 11. Tectonic discrimination diagrams of the Daga pluton (a-b from Pearce et al., 1984; c from Muller and Groves, 1994; d from Gorton and Schandl, 2000).

(2017) conclude that both the hornblende gabbro and the granite share a similar geodynamic setting and propose that the granite was likely formed by partial melting of lower crustal material derived from underplating basaltic magmas. By contrast, the hornblende-gabbro is probably the product of partial melting of metasomatized hydrous mantle in the Neo-Tethyan paleo-subduction zone. Based on these new data, Ma et al. (2017) propose the opening of the Neo-Tethys paleo-ocean during the late Permian. Recently, Wang et al. (2016) report zircon U-Pb age and Hf isotope data, whole-rock geochemistry and Sr-Nd isotopic data from Middle-Late Triassic volcanic rocks (andesitic and basaltic rocks) in the southernmost Lhasa terrane (Fig. 1b). Based on those data, Wang et al. (2016) propose that the northward subduction of the Neo-Tethys oceanic seafloor beneath the Lhasa terrane commenced before the Middle Triassic.

Moreover, there is also evidence from sedimentary, stratigraphic and paleomagnetic data suggesting that the birth of the Neo-Tethys paleo-ocean occurred prior to Late Triassic. For example, abundant Triassic detrital zircons

(240–210 Ma) collected from the Takena and the Duoba Formations as well as the Chumulong Formation are documented (Leier et al., 2007). Additionally, Hu et al. (2016) propose that in the Tethys-Himalaya region, the western Himalaya sedimentary succession is similar to that of southern Tibet in its upper part, indicating that the birth of the Neo-Tethys might have commenced already earlier than previously anticipated. Late Triassic metaflysch units, widely distributed in southern Tibet, are usually considered to be sediments of the passive continental margin of the Neo-Tethys Ocean (Sun Honglie and Zhang Du, 1998).

Based on paleomagnetic studies, Li Pengwu et al. (2005) conclude that the Neo-Tethys paleo-ocean had formed before the Late Triassic. More specifically, Chen et al. (2012) propose that the width of the Neo-Tethys paleo-ocean extended over 6000 kilometers during the Late Jurassic-Early Cretaceous. Considering the large paleo-distance between the Himalaya and the Neo-Tethys Ocean, Yang et al. (2015) infer that the Neo-Tethys Ocean was situated between the Himalaya and the Lhasa terrane

and its original width measured approximately 7000 ± 650 km at about 134–130 Ma ago. Data from Yang et al. (2015) is consistent with Chen et al. (2012) and their conclusion. Both studies suggest that the Neo-Tethys paleo-ocean had existed over a long time period since at least Early Triassic.

In summary, we propose that the late Triassic magmatism in the Gangdese belt was potentially related to the northward subduction of the Neo-Tethys oceanic crust beneath the Lhasa terrane. A simple tectonic sketch map of the tectonic evolution of the southern Tibet during the Late Triassic is shown in Fig. 12.

6 Conclusions and Geodynamic Implications for Southern Tibet

After discussing the previous studies on the pre-

Cretaceous magmatism in the Gangdese belt, we propose the following geodynamic model to explain all available data.

The zircon Hf isotopic mapping demonstrates that the Lhasa terrane can be divided into three different segments, the south Lhasa sub-terrane, the central Lhasa sub-terrane and the north Lhasa sub-terrane (Hou Zengqian et al., 2008; Zhu et al., 2011; Zhang Lixue et al., 2013). The divisions of the Hf isotopic mapping are consistent with data from Mo Xuanxue et al. (2009) and Zhu et al. (2011) also suggesting the presence of regional faults and tectonic mélanges (Fig. 1a). Both the southern and the northern Lhasa sub-terrane include contributions of juvenile crust as revealed by positive $\varepsilon_{\text{Hf}}(t)$ values and young two-stage model ages which indicate crustal growth. However, the central Lhasa sub-terrane is characterized by negative $\varepsilon_{\text{Hf}}(t)$ values and old model ages, suggesting the recycling of

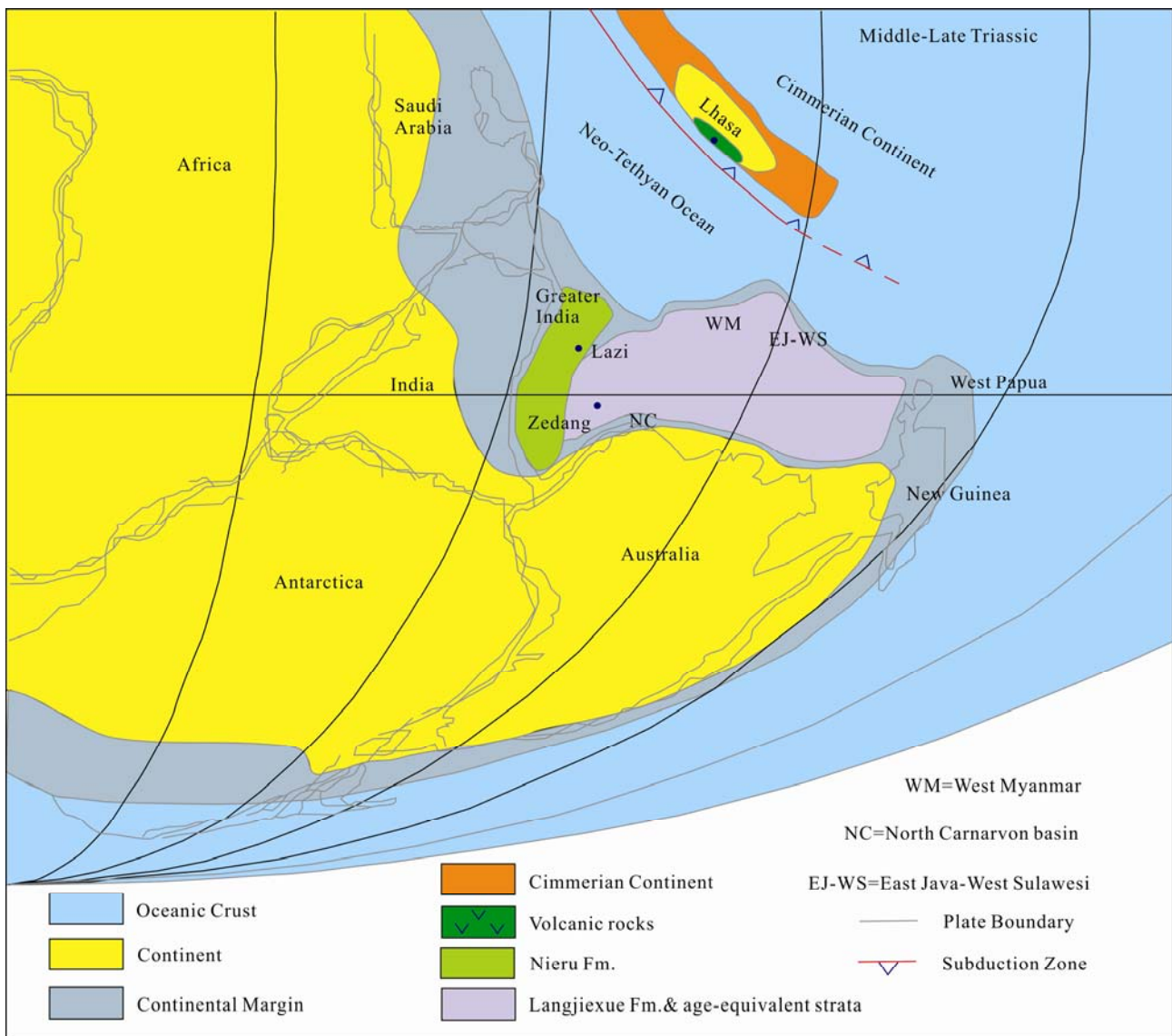


Fig. 12. Simplified Middle-Late Triassic paleo-geographic reconstruction of the Neo-Tethyan margin (modified from Cai et al., 2016).

ancient crust (Zhu et al., 2011). The Hf isotopic mapping of the Lhasa terrane provides strong evidence that the central Lhasa sub-terrane represents a microcontinent containing ancient basement (Xu Wangchun, 2010; Zhu et al., 2011; Zhu Dicheng et al., 2012; Zhang Lixue et al., 2013). In the period of Late Permian to Early- to Middle Triassic, the Yarlung Tsangpo rifting commenced (Pan et al., 2012; Meng et al., 2016a). Related deep-sea sediments also support this interpretation, such as the Ladinian-Carnian radiolaria chert and sedimentary sequences, witnessing the formation of the Neo-Tethys oceanic basin (Sun Honglie and Zhang Du, 1998; He Zhonghua et al., 2005, 2006; Zhu Jie et al., 2006). During Late Triassic and Early Jurassic, the northward subduction of the Neo-Tethys oceanic lithosphere occurred, producing the Late Triassic and Early Jurassic magmatism of southern Tibet (He Zhonghua et al., 2005, 2006; Ji et al., 2009; Peng Jianhua et al., 2013; Kang et al., 2014; Song Shaowei et al., 2014; Qiu Jiansheng et al., 2015; Meng et al., 2016a, b; Wang et al., 2016; Ma et al., 2017; and references therein). During the early period of the Neo-Tethys oceanic subduction, the Gangdese batholith was still relatively small. The igneous rocks have highly positive $\varepsilon_{\text{Hf}}(t)$ values, plotting along the depleted mantle line or in its vicinity (Fig. 9a). Although some granite samples have S-type signatures, they also have highly positive $\varepsilon_{\text{Hf}}(t)$ values (Ji et al., 2009; Xu Wangchun, 2010; Ma et al., 2017), indicating their derivation from juvenile crust nor ancient sediments or basement. Based on the Hf isotope mapping, we infer that the Gangdese belt, namely the southern Lhasa sub-terrane represents a tectonic amalgamation with the Lhasa microcontinent (central Lhasa sub-terrane) from Late Triassic to Early Middle Jurassic. During Late Jurassic and Early Cretaceous, the magmatic activity was relatively weak, resulting in a magmatic gap in southern Tibet, which is attributed to flat subduction of the Neo-Tethys oceanic slab. By contrast, there is a widespread magmatism in southern Tibet between Late Jurassic (152 Ma) and the Early Cretaceous (109 Ma) based on detrital zircon ages and Hf isotope studies on the Xigaze Group (Wu et al., 2010). The complex tectonic framework of the numerous terranes, subduction zones and post-collisional arcs explains some of the previous controversies. The subduction of the Neo-Tethys oceanic slab has generated arc-related granitic magmas, marked by LREE enrichments and depletions in HREE and HFSE (Nb, Ta and Ti) as well as I-type signatures (Figs. 5–6). Those geochemical signatures have a good consensus with sedimentary and paleo-magnetic data.

In summary, the Daga pluton in the Quxu region of southern Tibet was emplaced during the beginning of Late

Triassic (225–229 Ma). Its geochemical and Hf isotopic characteristics suggest that the Daga pluton was derived from the partial melting of juvenile crust, but mixed with underplated mantle material in a continental arc setting. Our data in addition to published data reveal that the Neo-Tethys paleo-ocean had formed already before the Triassic.

Acknowledgments

We appreciate the thorough and constructive comments by the reviewers and the editor-in-chief that greatly improved the presentation of this paper. Besides, we are grateful to Dr. Daniel Müller for his constructive reviews, which greatly helped us to improve the manuscript. We thank my collaborators and Tibetan drivers, whose selfless assistance enabled our geological field work possible. Many thanks go to Dingsheng Jiang for assisting in the zircon U-Pb dating and Lu-Hf isotopic analyses. This study was supported by the China Postdoctoral Science Foundation (M2017612220) and the Shandong Province Natural Science Foundation (Doctoral Funds, ZR2017BD033).

Manuscript received July 1, 2017

accepted Sept. 13, 2017

edited by Fei Hongcai

References

- Altherr, R., Holl, A., and Hegner, E., 2000. High-potassium, calc-alkaline I-type plutonism in the European Variscides, Northern Vosges (France) and northern Schwarzwald (Germany). *Lithos*, 50: 51–73.
- Anthony, E.Y., 2005. Source regions of granites and their links to tectonic environment, Examples from the western United States. *Lithos*, 80 (1–4): 61–74.
- Barbarin, B., 1990. Granitoids, main petrogenetic classification in relation to origin and tectonic setting. *Geological Journal*, 25: 227–238.
- Barbarin, B., 1999. A review of the relationships between granitoid types, their origins and their geodynamic environments. *Lithos*, 46: 605–626.
- Boynton, W.V., 1984. *Geochemistry of the rare earth elements, Meteorite studies*, in Henderson, P., ed., *Rare earth element geochemistry*. Amsterdam: Elsevier, 63–114.
- Cai, F., Ding, L., Laskowski, A.K., Kapp, P., Wang, H., Xu, Q., and Zhang, L., 2016. Late Triassic paleogeographic reconstruction along the Neo-Tethyan Ocean margins, southern Tibet. *Earth and Planetary Science Letters*, 435: 105–114.
- Cen Kuang and Chen Yuan, 2011. The ordering mode of geochemical differentiation index of elements in continental crust. *Earth Science Frontier*, 18(1): 56–62 (in Chinese with English abstract).
- Chappell, B.W., 1999. Aluminium saturation in I- and S-type granites and the characterization of fractionated haplogranites.

- Lithos*, 46(3): 535–551.
- Chappell, B.W., Bryant, C.J., Wyborn, D., White, A.J.R., and Williams, I.S., 1998. High- and low-temperature I-type granites. *Resource Geology*, 48(4): 225–235.
- Chen Tao, 2006. *Geochemistry of the Qushui intrusive of Gangdese in Tibet and its implications for magma mixing*. Beijing: China University of Geosciences (Master thesis): 1–57 (in Chinese with English Abstract).
- Chen, W.W., Yang, T.S., Zhang, S.H., Yang, Z.Y., Li, H.Y., Wu, H.C., Zhang, J.H., and Ma, Y.M., 2012. Paleomagnetic results from the Early Cretaceous Zenong Group volcanic rocks, Cuoqin, Tibet, and their paleogeographic implications. *Gondwana Research*, 22(2): 461–469.
- Chu, M.F., Chung, S.L., Song, B.A., Liu, D.Y., O'Reilly, S.Y., Pearson, N.J., Ji, J.Q., and Wen, D.J., 2006. Zircon U-Pb and Hf isotope constraints on the Mesozoic tectonics and crustal evolution of southern Tibet. *Geology*, 34 (9): 745–748.
- Chung, S.L., Chu, M.F., Zhang, Y.Q., Xie, Y.W., Lo, C.H., Lee, T.Y., Lan, C.Y., Li, X.H., Zhang, Q., and Wang, Y.Z., 2005. Tibetan tectonic evolution inferred from spatial and temporal variations in post-collisional magmatism. *Earth-Science Reviews*, 68: 173–196.
- Chung, S.L., Liu, D., Ji, J.Q., Chu, M.F., Lee, H.Y., Wen, D.J., Lo, C.H., Lee, T.Y., Qian, Q., and Zhang, Q., 2003. Adakites from continental collision zones, melting of thickened lower crust beneath southern Tibet. *Geology*, 31: 1021–1024.
- Condie, K.C., 1982. *Plate tectonics and crustal evolution*. New York: Pergamon, 1–310.
- de Hollanda, M.H.B.M., Pimentel, M.M., and Sá, E.F.J., 2003. Paleoproterozoic subduction related metasomatic signatures in the lithospheric mantle beneath NE Brazil: inferences from trace element and Sr-Nd-Pb isotopic compositions of Neoproterozoic high-K igneous rocks. *Journal of South American Earth Sciences*, 15: 885–900.
- Dong Guochen, Mo Xuanxue, Zhao Zhidan, Guo Tiejing, Wang Liangliang and Chen Tao, 2005. Geochronologic constraints by SHRIMP II zircon U-Pb dating on magma underplating in the Gangdese belt following India-Eurasia collision. *Acta Geologica Sinica* (English Edition), 79(6): 784–794.
- Dong Xin and Zhang Zeming, 2013. Genesis and tectonic significance of the Early Jurassic magmatic rocks from the southern Lhasa terrane. *Acta Petrologica Sinica*, 29(6): 1933–1948 (in Chinese with English abstract).
- Foley, S.F., and Wheller, G.E., 1990. Parallels in the origin of the geochemical signatures of island arc volcanics and continental potassic igneous rocks, the role of residual titanates. *Chemical Geology*, 85(1–2): 1–18.
- Gao Jianfeng, Lu Jianjun, Lai Mingyuan, Lin Yuping and Pu Wei, 2003. Analysis of trace elements in rock samples using HR-ICPMS. *Journal of Nanjing University* (Natural Sciences), 39 (6): 844–850 (in Chinese with English abstract).
- Geng Quanru, Pan Guitang, Wang Liquan, Zhu Dicheng and Liao Zhongli, 2006. Isotopic geochronology of the volcanic rocks from the Yeba formation in the Gangdese zone, Xizang. *Sedimentary Geology and Tethyan Geology*, 26(1): 1–7 (in Chinese with English abstract).
- Goolaerts, A., Mattielli, N., Jong, J.D., Weis, D., and Scoates, J., 2004. Hf and Lu isotopic reference values for the zircon standard 91500 by MC-ICP-MS. *Chemical Geology*, 206(1–2): 1–9.
- Gorton, M.P., and Schandl, E.S., 2000. From continents to island arcs, a geochemical index of tectonics setting for arc-related and within-plate felsic to intermediate volcanic rocks. *The Canadian Mineralogist*, 38(5): 1065–1073.
- Griffin, W.L., Belousova, E.A., Shee, S.R., Pearson, N.J., and O'Reilly, S.Y., 2004. Archean crustal evolution in the northern Yilgarn Craton: U-Pb and Hf - isotope evidence from detrital zircons. *Precambrian Research*, 131(3): 231–282.
- He Zhonghua, Yang Deming, Zheng Changqing and Huang Yingcong, 2005. Geochemistry of the Indosinian granitoids in the Mamba area, Gangdise belt, Tibet and its tectonic significance. *Geological Bulletin of China*, 24(4): 354–359 (in Chinese with English abstract).
- He Zhonghua, Yang Deming, Zheng Changqing and Wang Tianwu, 2006. Isotopic dating of the Mamba granitoid in the Gangdese tectonic belt and its constraint on the subduction time of the Neo-Tethys. *Geological Review*, 52(1): 100–106 (in Chinese with English abstract).
- Hoskin, P.W.O., and Schaltegger, U., 2003. The composition of zircon and igneous and metamorphic petrogenesis. *Reviews in Mineralogy and Geochemistry*, 53: 27–62.
- Hou Zengqian, Wang Erchie, Mo Xuanxue, Ding Lin, Pan Guitang and Zhang Zhongjie, 2008. *Collisional orogeny and metallogenesis of the Tibetan plateau*. Beijing: Geological Publishing House, 1–980 (in Chinese).
- Hu, X., Garzanti, E., Wang, J., Huang, W., An, W., Webb, A., 2016. The timing of India-Asia collision onset-facts, theories, controversies. *Earth-Science Reviews*, 160: 264–299.
- Huang Yong, Li Guangming, Ding Jun, Dai Jie, Yan Guoqiang, Don Suiliang and Huang Hanxiao, 2017. Origin of the newly discovered Zhunuo porphyry Cu-Mo-Au deposit in the western part of the Gangdese porphyry copper belt in the southern Tibetan plateau, SW China. *Acta Geologica Sinica* (English Edition), 91(1): 109–134.
- Huang Yu, Zhao Zhidan, Zhang Fengqin, Zhu Dicheng, Dong Guochen, Zhou Su and Mo Xuanxue, 2010. Geochemistry and implication of the Gangdese batholiths from Renbu and Lhasa areas in southern Tibet. *Acta Petrologica Sinica*, 26(10): 3131–3142 (in Chinese with English abstract).
- Jackson, S.E., Pearson, N.J., Griffin, W.L., and Elousova, E.A., 2004. The application of laser ablation-inductively coupled plasma-mass spectrometry to in situ U-Pb zircon geochronology. *Chemical Geology*, 211(1): 47–69.
- Ji Weiqiang, Wu Fuyuan, Chung Sunglin and Liu Chuazhou, 2009. Geochronology and petrogenesis of granitic rocks in Gangdese batholith, southern Tibet. *Science in China: Series D Earth Sciences*, 52(9): 1240–1261.
- Ji, W.Q., Wu, F.Y., Chung, S.L., Li, J.X., and Liu, C.Z., 2009. Zircon U-Pb geochronology and Hf isotopic constraints on petrogenesis of the Gangdese batholith, southern Tibet. *Chemical Geology*, 262: 229–245.
- Jin Chengwei and Zhou Yunsheng, 1978. Igneous rock belts in the Himalayas and the Gangdese arc and their genetic model. *Scientia Geologica Sinica*, 4: 297–312 (in Chinese with English abstract).
- Jogvan, O., Muntener, O., Burg, J.P., Ulmer, P., and Jagoutz, E., 2006. Lower continental crust formation through focused flow in km-scale melt conduits: The zoned ultramafic bodies of the Chilas complex in the Kohistan island arc (NW Pakistan). *Earth and Planetary Science Letters*, 242 (3–4): 320–342.
- Kang, Z.Q., Xu, J.F., Wilde, S.A., Feng, Z.H., Chen, J.L., Wang, B.D., Fu, W.C., and Pan, H.B., 2014. Geochronology and

- geochemistry of the Sangri Group volcanic rocks, southern Lhasa terrane, implications for the Early subduction history of the Neo-Tethys and Gangdese magmatic arc. *Lithos*, 200–201: 157–168.
- Kelemen, P.B., Johnson, K.T.M., Kinzler, R.J., and Irving, A.J., 1990. High-field-strength element depletions in arc basalts due to mantle-magma interaction. *Nature*, 345 (6275): 521–524.
- Leier, A.L., Decelles, P.G., Kapp, P., and Gehrels, G.E., 2007. Lower Cretaceous Strata in the Lhasa Terrane, Tibet, with implications for understanding the early tectonic history of the Tibetan Plateau. *Journal of Sedimentary Research*, 77(9–10): 809–825.
- Li Cai, 1987. The Longmuco–Shuanghu–Lancangjiang Plate suture and the north boundary of distribution of Gondwana facies Permo–Carboniferous system in northern Xizang, China. *Journal of Changchun College of Geology*, 17(2): 155–166 (in Chinese with English abstract).
- Li Huaqi, 2009. *The geological significance of Indosinian Orogenesis occurred in Lhasa Terrane*. Beijing: Chinese Academy of Geological Sciences (Ph.D thesis): 1–109 (in Chinese with English abstract).
- Li Pengwu, Gao Rui, Cui Junwen and Guan Ye, 2005. Paleomagnetic results from the three rivers region, SW China, Implications for the collisional and accretionary history. *Acta Geoscientica Sinica*, 26(5): 387–404 (in Chinese with English abstract).
- Ludwig, K.R., 2001. *Isoplot—A Geochronological Toolkit for Microsoft Excel*. Berkeley Geochronology Center Special Publication No. 1a, 1–58.
- Ma, S.W., Meng, Y.K., Xu, Z.Q., and Liu, X.J., 2017. The discovery of late Triassic mylonitic granite and geologic significance in the middle Gangdese batholiths, southern Tibet. *Journal of Geodynamics*, 104: 49–64.
- Ma, X.X., Xu, Z.Q., and Meert, J.G., 2016. Eocene slab breakoff of Neotethys as suggested by dioritic dykes in the Gangdese magmatic belt, southern Tibet. *Lithos*, 248–251: 55–65.
- Maniar, P.D., and Piccoli, P.M., 1989. Tectonic discrimination of granitoids. *Geological society of America bulletin*, 101(5): 635–643.
- Meng, Y.K., Xu, Z.Q., Santosh, M., Ma, X.X., Chen, X.J., Guo, G.L., and Liu, F., 2016a. Late Triassic crustal growth in southern Tibet, evidence from the Gangdese magmatic belt. *Gondwana Research*, 37: 449–464.
- Meng, Y.K., Dong, H.W., Cong, Y., Xu, Z.Q., and Cao, H., 2016b. The early-stage evolution of the Neo-Tethys ocean, Evidence from granitoids in the middle Gangdese batholith, southern Tibet. *Journal of Geodynamics*, 94–95: 34–49.
- Meng Yuanku, Xu Zhiqin, Ma Shiwei and Yang Feifei, 2016a. The ^{40}Ar - ^{39}Ar geochronological constraints on the Xaitongmoin-Quxu ductile shear zone in the Gangdese batholith, southern Xizang (Tibet). *Geological Review*, 62(4): 795–806 (in Chinese with English abstract).
- Meng Yuanku, Xu Zhiqin, Ma Shiwei and Liu Xiaojia, 2016b. Application of the Kinematic Vorticity in the Xaitongmoin-Quxu Ductile Shear Zone in the Middle Gangdese Magmatic Belt, Southern Tibet. *Acta Geologica Sinica*, 90(11): 3023–3038 (in Chinese with English abstract).
- Middlemost, E.A.K., 1994. Naming materials in the magma/igneous rock system. *Earth-Science Reviews*, 37: 215–224.
- Mo Xuanxue, 2011. Magmatism and evolution of the Tibetan plateau. *Geological Journal of China Universities*, 17(3): 351–367 (in Chinese with English abstract).
- Mo Xuanxue, Dong Guochen, Zhao Zhidan, Zhou Su, Wang Liangliang, Qiu Ruizhao and Zhang Fengqin, 2005a. Spatial and temporal distribution and characteristics of granitoids in the Gangdese, Tibet and Implication for crustal growth and evolution. *Geological Journal of China Universities*, 11(3): 281–290 (in Chinese with English abstract).
- Mo Xuanxue, Dong Guochen, Zhao Zhidan, Guo Tiejing, Wang Liangliang and Chen Tao, 2005b. Timing of magma mixing in the Gangdise magmatic belt during the India-Asia collision, zircons SHRIMP U-Pb dating. *Acta Geologica Sinica* (English Edition), 79(1): 66–76.
- Mo, X.X., Niu, Y.L., Dong, G.C., Zhao, Z.D., Hou, Z.Q., Zhou, S., and Ke, S., 2008. Contribution of syn-collisional felsic magmatism to continental crust growth, a case study of the Paleogene Linzizong volcanic succession in southern Tibet. *Chemical Geology*, 250(1–4): 49–67.
- Mo Xuanxue, Zhao Zhidan, Deng Jinfu, Dong Guochen, Zhou Su, Guo Tingying, Zhang Shuangquan and Wang Liangliang, 2003. Response of volcanism to the India-Asia collision. *Earth Science Frontiers*, 10(3): 135–148 (in Chinese with English abstract).
- Mo Xuanxue, Zhao Zhidan, Yu Xuehui, Dong Guochen, Li Youguo, Zhou Su, Liao Zhongli and Zhu Dicheng, 2009. *Cenozoic Collisional-Post-collisional Igneous Rocks in the Tibetan Plateau*. Beijing: Geological Publishing House, 1–380 (in Chinese).
- Muller, D., and Groves, D.I., 1994. *Potassic igneous rocks and associated gold-copper mineralization*. Lect. Notes Earth Sci., 56.
- Pan, G.T., Wang, L.Q., Li, R.S., Yuan, S.H., Ji, W.H., Yin, F.G., Zhang, W.P., and Wang, B.D., 2012. Tectonic evolution of the Qinghai-Tibet Plateau. *Journal of Asian Earth Sciences*, 53: 3–14.
- Patino Douce, A.E., 1999. What do experiments tell us about the relative contributions of crust and mantle to the origin of granitic magmas? In: Castro, A., Fernandez, C., and Vigneresse, J.L. (eds.), *Understanding Granites, Integrating New and Classical Techniques*. Geological Society, London, Special Publications, 168: 55–75.
- Patino Douce, A.E., and Beard, J.S., 1996. Effects of P, f(O₂) and Mg/Fe ratio on dehydration melting of model metagreywackes. *Journal of Petrology*, 37(5): 999–1024.
- Patino Douce, A.E., McCarthy, T.C., 1998. Melting of crustal rocks during continental collision and subduction. In: Hacker, B.R., and Liou, J.G. (eds.), *When Continents collide, Geodynamics and Geochemistry of Ultrahigh-Pressure Rocks. Petrology and Structural Geology*. Dordrecht, Kluwer Academic Publishers, 10: 27–55.
- Pearce, J.A., Harris, N.B., and Tindle, A.G., 1984. Trace element discrimination diagrams for the tectonic interpretation of granitic rocks. *Journal of Petrology*, 25: 956–983.
- Pearce, J.A., and Peate, D.W., 1995. Tectonic implications of the composition of volcanic arc magmas. *Annual Review of Earth and Planetary Sciences*, 23(1): 251–285.
- Peccerillo, A., and Taylor, S.R., 1976. Geochemistry of Eocene calc-alkaline volcanic rocks from the Kastamonu area, northern Turkey. *Contributions to Mineralogy and Petrology*, 58: 63–81.
- Peng Jianhua, Zhao Xiliang, He Jun, Huang Shaochun and Gong

- Chen, 2013. Discovery of Indosinian Magmatic Rocks and Its significance in Western Gangdise, Tibet. *Journal of East China Institute of Technology (Natural Science)*, 36(s2): 21–26 (in Chinese with English abstract).
- Perfit, M.R., Gust, D.A., Bence, A.E., Arculus, R.J., and Taylor, S.R., 1980. Chemical characteristics of island-arc basalts, implications for mantle sources. *Chemical Geology*, 30(3): 227–256.
- Pitcher, W.P., 1979. The nature, ascent and emplacement of granitic magmas. *Journal of the Geological Society*, 136(6): 627–662.
- Qiu Jiansheng, Wang Ruiqiang, Zhao Jiaolong and Yu Sibin, 2015. Petrogenesis of the Early Jurassic gabbro-granite complex in the middle segment of the Gangdese belt and its implications for tectonic evolution of Neo-Tethys: A case study of the Dongga pluton in Xi'gaze. *Acta Petrologica Sinica*, 31(12): 3569–3580 (in Chinese with English abstract).
- Rapp, R.P., and Watson, E.B., 1995. Dehydration melting of meta-basalt at 8–32kbar, Implications for continental growth and crust–mantle recycling. *Journal of Petrology*, 36: 891–931.
- Rapp, R.P., Watson, E.B., and Miller, C.F., 1991. Partial melting of amphibolite/eclogite and the origin of Archean trondhjemitic and tonalities. *Precambrian Research*, 51(1–4): 1–25.
- Saunders, A.D., Tarney, J., and Weaver, S.D., 1980. Transverse geochemical variations across the Antarctic Peninsula, implications for the genesis of calc–alkaline magmas. *Earth and Planetary Science Letters*, 46: 344–360.
- Skjerlie, K.P., and Douce, A.E.P., 2002. The fluid–absent partial melting of a zoisite–bearing quartz eclogite from 1.0 to 3.2GPa, implications for melting in thickened continental crust and for subduction–zone processes. *Journal of Petrology*, 43: 291–314.
- Song Shaowei, Liu Ze, Zhu Dicheng, Wang Qing, Zhang Lixiang, Zhang Liangliang and Zhao Zhidan, 2014. Zircon U–Pb chronology and Hf isotope of the Late Triassic andesitic magmatism in Dajiacuo, Tibet. *Acta Petrologica Sinica*, 30 (10): 3100–3112 (in Chinese with English Abstract).
- Sun Honglie and Zheng Du, 1998. *Formation evolution and development of Qinghai-Xizang (Tibetan) plateau*. Guangzhou: Guangdong Science Press, 41–44 (in Chinese).
- Sun, S.S., and McDonough, W.F., 1989. Chemical and isotopic systematics of oceanic basalts, Implications for mantle composition and processes. In: Saunders, A.D., and Norry, M.J. (eds.), *Magmatism in the ocean basins*. Geological Society, London: Special Publications, 42: 313–345.
- Tu Guangchi, Zhang Yuquan, Zhao Zhenhua and Wang Zhonggang, 1981. Characteristics and evolution of granitoids of south Xizang (Tibet). *Geochimica*, 1, 1–7 (in Chinese with English abstract).
- Vervoort, J., and Blichert–Toft, J., 1999. Evolution of the depleted mantle, Hf isotope evidence from juvenile rocks through time. *Geochimica et Cosmochimica Acta*, 63(3–4): 533–556.
- Wang, C., Ding, L., Zhang, L. Y., Kapp, P., Pullen, A., and Yue, Y. H., 2016. Petrogenesis of middle–late triassic volcanic rocks from the Gangdese belt, southern Lhasa terrane, Implications for early subduction of Neo–Tethyan oceanic lithosphere. *Lithos*, 262: 320–333.
- Wang Cheng, Wei Qirong, Liu Xiaonian, Ding Pengfei, Bu Tao, Sun Ji, Zhang Xiaoqiang and Wang, Jingyuan, 2014. Post-Collision related Late Indosinian granites of Gangdise Terrane: Evidences from zircon U–Pb Geochronology and Petrogeochemistry. *Earth Sciences–Journal of China University of Geosciences*, 39(9): 1277–1300 (in Chinese with English abstract).
- Wang, R., Richards, J.P., Zhou, L.M., Hou, Z.Q., Stern, R.A., Creaser, R.A., and Zhu, J.J., 2015. The role of Indian and Tibetan lithosphere in spatial distribution of Cenozoic magmatism and porphyry Cu–Mo deposits in the Gangdese belt, southern Tibet. *Earth Science Reviews*, 150: 68–94.
- Wang Tao, Wang, X.X., Guo, L., Zhang, L., Tong, Y., Li, S., Huang, H., and Zhang, J.J., 2017. Granitoid and tectonics. *Acta Petrologica Sinica*, 33(5): 1459–1478 (in Chinese with English abstract).
- Wen, D. R., Liu, D., Chung, S. L., Chu, M. F., Ji, J., Song, B., Lee, T.Y., Yeh, M.W., and Lo, C.H., 2008. Zircon SHRIMP U–Pb ages of the Gangdese batholith and implications for Neotethyan subduction in southern Tibet. *Chemical Geology*, 252(3–4): 191–201.
- Winter, J.D., 2001. *An introduction to igneous and metamorphic petrology*. New Jersey: Prentice Hall, 1–697.
- Winther, K.T., 1996. An experimentally based model for the origin of tonalitic and trondhjemitic melts. *Chemical Geology*, 127 (1–3): 43–59.
- Wolf, M.B., and Wyllie, J.P., 1994. Dehydration–melting of amphibolite at 10kbar, the effects of temperature and time. *Contributions to Mineralogy and Petrology*, 115 (4): 369–383.
- Wu, F.Y., Ji, W.Q., Liu, C.Z., and Chung, S.L., 2010. Detrital zircon U–Pb and Hf isotopic data from the Xigaze fore–arc basin, Constraints on Transhimalayan magmatic evolution in southern Tibet. *Chemical Geology*, 271(1–2): 13–25.
- Wu Fuyuan, Li Xianhua, Zheng Yongfei and Gao Shan, 2007. Lu–Hf isotopic systematics and their applications in petrology. *Acta Petrologica Sinica*, 23(2): 185–220 (in Chinese with English abstract).
- Wu Yuanbao and Zheng Yongfei, 2004. Genesis of zircon and its constraints on interpretation of U–Pb age. *Chinese Science Bulletin*, 49(15): 1554–1569.
- Xu Bo, Hou Zengqian, Zheng Yuanchuan, Zhou Ye, Zhou Limin, Yang Yu, Han Yanwei, Guo Zhen and Wu Changda, 2017. Jurassic hornblende gabbros in Dongga, eastern Gangdese, Tibet: partial melting of mantle wedge and implications for crustal growth. *Acta Geologica Sinica (English Edition)*, 91(2): 545–564.
- Xu Ronghua and Jin Chengwei, 1984. A geochronological study the Quxu batholith, Xizang. *Scientia Geologica Sinica*, 4: 414–422 (in Chinese with English abstract).
- Xu Wangchun, 2010. *Spatial variation of zircon U–Pb ages and Hf isotopic compositions of the Gangdese granitoids and its geologic implications*. Wuhan: China University of Geosciences (Ph. D thesis): 1–96 (in Chinese with English Abstract).
- Xu, W.C., Zhang, H.F., Luo, B.J., Guo, L., and Yang, H., 2015. Adakite–like geochemical signature produced by amphibole–dominated fractionation of arc magmas, An example from the Late Cretaceous magmatism in Gangdese belt, south Tibet. *Lithos*, 232: 197–210.
- Xu Xisheng and Qiu Jiansheng, 2010. *Igneous Petrology*. Beijing: Science Press, 1–346 (in Chinese).

- Xu Zhiqin, Yang Jingsui, Li Haibing, Ji Shaocheng, Zhang Zeming and Liu Yan, 2011. On the tectonics of India–Asia collision. *Acta Geologica Sinica*, 85(1): 1–33 (in Chinese with English abstract).
- Yang, J.S., Xu, Z.Q., Li, Z.L., Xu, X.Z., Li, T.F., Ren, Y.F., Li, H.Q., Chen, S.Y., and Robinson, P.T., 2006. Discovery of an eclogite belt in the Lhasa block, Tibet, A new border for Paleo–Tethys? *Journal of Asian Earth Sciences*, 34(1): 76–89.
- Yang, T.S., Ma, Y.M., Bian, W.W., Jin, J.J., Zhang, S.H., Wu, H.C., Li, H.X., Yang, Z.Y., and Ding, J.K., 2015. Paleomagnetic results from the early Cretaceous Lakang formation lavas, constraints on the paleolatitude of the Tethyan Himalaya and the India–Asia collision. *Earth and Planetary Science Letters*, 428: 120–133.
- Yin, A., and Harrison, T.M., 2000. Geologic evolution of the Himalayan–Tibetan orogen. *Annual Review of Earth and Planetary Sciences*, 28: 211–280.
- Zhang Hongfei, Xu Wangchun, Guo Jianqiu, Zong Keqing, Cai Hongming and Yuan Honglin, 2007. Indosinian Orogenesis the Gangdise Terrane, Evidences from Zircon U–Pb Dating and Petrogenesis of Granitoids. *Earth Science–Journal of China University of Geosciences*, 32(2): 155–166 (in Chinese with English abstract).
- Zhang Lixue, Wang Qing, Zhu Dicheng, Jia Lili, Wu Xingyuan, Liu Shengao, Hu Zhaochu and Zhao Tianpei, 2013. Mapping the Lhasa terrane through zircon Hf isotopes, Constraints on the nature of the crust and metallogenic potential. *Acta Petrologica Sinica*, 29(11): 3681–3688 (in Chinese with English abstract).
- Zhang, Z.M., Ding, L., Zhao, Z.D., and Santosh, M., 2017. Tectonic evolution and dynamics of the Tibetan Plateau. *Gondwana Research*, 41: 1–8.
- Zhu, D.C., Wang, Q., Zhao, Z. D., Chung, S. L., Cawood, P. A., Niu, Y.L., Liu, S.A., Wu, F.Y., and Mo, X.X., 2015. Magmatic record of India–Asia collision. *Scientific Reports* 5, 14289; Doi, 10.1038/srep14289.
- Zhu, D.C., Zhao, Z.D., Niu, Y.L., Mo, X.X., Chung, S.L., Hou, Z.Q., Wang, L.Q and Wu, F.Y., 2011. The Lhasa terrane, record of microcontinent and its histories of drift and growth. *Earth and Planetary Science Letter*, 301: 241–255.
- Zhu Dicheng, Zhao Zhidan, Niu Yaoling, Wang Qing, Yildirim D, Dong Guochen and Mo Xuanxue, 2012. Origin and Paleozoic tectonic evolution of the Lhasa terrane. *Geological Journal of China Universities*, 18(1): 1–15 (in Chinese with English abstract).
- Zhu Jie, Du Yuansheng, Liu Zaoxue, Feng Qinglai and Tian Wangxue, Li Jinping and Wang Changping, 2006. Mesozoic radiolarian chert from the middle sector of the Yarlung Zangbo suture zone, Tibet and its tectonic implications. *Science in China, Series D Earth Sciences*, 49(4): 348–357.
- Zorpi, M.J., Coulon, C., and Orsini, J.B., 1991. Hybridization between felsic and mafic magmas in calc-alkaline granitoids—a case study in northern Sardinia, Italy. *Chemical Geology*, 92: 45–86.

About First author:

MENG Yuanku, male, a postdoctoral researcher at the Qingdao Institute of Marine Geology, China Geological Survey. Recently, He focuses on marine geology and Tibetan geology, including tectonics, structural deformations and sedimentary setting analyses. E-mail address: ykmeng@foxmail.com; phone: +8615563459838.